The endosymbiotic origins of the apicoplast link fever-survival and artemisinin-resistance in the malaria parasite

Min Zhang[a,1], Chengqi Wang[a,1], Jenna Oberstaller[a,1], Phaedra Thomas[a], Thomas D. Otto[b,c], Debora Casandra[a], Sandhya Boyapalle[a], Swamy R. Adapa[a], Shulin Xu[a], Katrina Button-Simons[d], Matthew Mayho[b], Julian C. Rayner[b,e], Michael T. Ferdig[e], Rays H. Y. Jiang[a], John H. Adams[a,2]

[a]Center for Global Health and Infectious Diseases Research and USF Genomics Program, College of Public Health, University of South Florida, 3720 Spectrum Blvd, Suite 404, Tampa, Florida 33612, USA

[b]Wellcome Sanger Institute, Wellcome Genome Campus, Hinxton Cambridgeshire, CB10 1SA United Kingdom

[c]Institute of Infection, Immunity and Inflammation, MVLS, University of Glasgow, Glasgow G12 8TA United Kingdom

[d]Eck Institute for Global Health, Department of Biological Sciences, University of Notre Dame, Notre Dame, IN 46556

[e]Cambridge Institute for Medical Research, University of Cambridge, Cambridge Biomedical Campus, The Keith Peters Building, Hills Road, Cambridge, Cambridgeshire, CB2 0XY United Kingdom

[1] M.Z., C.W. and J.O. contributed equally to this work.

[2]To whom correspondence should be addressed. Email: ja2@usf.edu

ABSTRACT

Background: The emergence and spread of *Plasmodium falciparum* parasites resistant to front-line antimalarial artemisinin-combination therapies (ACT) threatens to erase the considerable gains against the disease of the last decade. We developed a new large-scale phenotypic screening pipeline and used it to carry out the first large-scale forward-genetic phenotype screen in *P. falciparum* to identify genes that allow parasites to survive febrile temperatures.

Results: Screening identified more than 200 *P. falciparum* mutants with differential responses to increased temperature. These mutants were more likely to be sensitive to artemisinin derivatives as well as to heightened oxidative stress. Major processes critical for *P. falciparum* tolerance to febrile temperatures and artemisinin included highly essential, conserved pathways associated with protein-folding, heat-shock and proteasome-mediated degradation, and unexpectedly, isoprenoid biosynthesis, which originated from the parasite's algal endosymbiont-derived plastid, the apicoplast. Apicoplast-targeted genes in general were up-regulated in response to heat shock, as were other *Plasmodium* genes with orthologs in plant and algal genomes.

Conclusions*:* *Plasmodium falciparum* parasites appear to exploit their innate febrile-response mechanisms to mediate resistance to artemisinin. Both responses depend on endosymbiotic cyanobacterium-related ancestral genes in the parasite's genome, suggesting a link to the evolutionary origins of *Plasmodium* parasites in free-living ancestors.

Running title: Plastid metabolism enables malaria parasites to survive fever and artemisinin

Key words: genome-wide phenotypic screens, *piggyBac,* QIseq, heat shock, growth fitness, transposon-mediated mutagenesis, phenotypic functional profiling

INTRODUCTION

Malaria remains a leading infectious disease causing >200 million clinical cases and a half-million deaths every year. *Plasmodium falciparum* is the deadliest malaria parasite by far, with growing parasite resistance to front-line antimalarial artemisinin-combination therapies (ACT) threatening to erase the considerable gains against the disease of the last decade. Alarmingly, data indicate that for the first time since 2010, progress in reducing global burden of malaria cases and fatalities nearly flatlined between 2015 and 2017 [1]. New therapies, ideally informed by an understanding of basic parasite biology, are needed to confront these urgent threats to global malaria control. The study of malaria-parasite biology and gene-function has traditionally been limited, because targeted gene-by-gene approaches are laborious and fraught with difficulty due to an AT-rich (~82%) genome that limits scalability of specific targeted gene-editing methods (such as CRISPR). Despite the considerable knowledge gene-by-gene studies have enabled, and the ~two decades that have passed since the *P. falciparum* genome was completed [2], the limited throughput of targeted gene-editing strategies combined with evolutionary distance of *P. falciparum* from classical model eukaryotes has left >90% of genes untouched experimentally, and ~35% of the parasite's ~5474 genes without meaningful functional annotation (www.plasmodb.org) [3]. High-throughput methods for functionally profiling the malaria-parasite genome can hasten development of effective interventions to control a parasite proven to be an adaptable foe.

Parasite-specific processes essential for parasite survival are naturally attractive as potential drug-targets, given the decreased likelihood of deleterious off-target effects to

78 the host. One such process ripe for interrogation is the parasite's survival-response to
79 the extreme conditions of the host's malarial fever. Repeating fever is a hallmark of all
80 types of malaria and the cyclical patterns serve as key diagnostic features of infections.
81 In malignant tertian malaria caused by *P. falciparum,* the 48-hour cycle corresponds to
82 the parasite's asexual intraerythrocytic-stage life-cycle, wherein parasites invade,
83 develop, asexually replicate and then rupture their host red blood cell (RBC) to begin the
84 destructive blood-stage cycle anew. Host fever is triggered by a Type I shock-like
85 response of the innate immune-system exposure to extracellular parasite debris
86 released when infected RBCs are lysed during parasite egress. Malarial fever
87 concomitantly attenuates and synchronizes development of blood-stage *P. falciparum*
88 infections, as it is lethal to all parasite stages except for early intraerythrocytic ring
89 stages. However, parasite tolerance of febrile temperatures is crucial for its successful
90 propagation in human populations as well as a fundamental aspect of malaria
91 pathogenesis. Previous research suggests parasite-specific factors play a role in
92 modulating this tolerance for febrile temperatures, though the identities of many of these
93 factors or the mechanisms by which they operate remain uncertain [4, 5].
94
95 We previously used random *piggyBac*-transposon insertional mutagenesis to uncover
96 genes essential for *P. falciparum* blood-stage survival, generating a saturation-level *P.*
97 *falciparum* mutant library containing ~38,000 single-disruption mutants [6]. We defined
98 2680 genes as essential for asexual blood-stage growth, including ~1000 *Plasmodium*-
99 conserved genes of unknown function. Here we demonstrate the potential of this
100 *piggyBac*-mutant (*pB*-mutant) library to systematically assign functional annotation to the
101 *P. falciparum* genome by genome-wide phenotypic screens. In this study, we present the
102 first large-scale forward-genetic functional screen in *P. falciparum* to identify factors
103 linked to parasite survival of febrile temperatures. Importantly, we functionally annotate

104 hundreds of parasite genes as critical for the parasite's response to heat shock (HS) but
105 dispensable under ideal growth-conditions, ~26% of which were previously unannotated
106 with no known function. Expression-profiling the HS-responses in two different heat
107 shock-sensitive (HS-Sensitive) *pB*-mutant clones vs. the wildtype parent NF54 via
108 RNAseq revealed concordance between (1) genes regulated in the parasite's innate
109 response to HS, (2) the processes dysregulated in these mutants vs. wildtype responses
110 to HS, and (3) those mutants we identified as HS-Sensitive in our pooled screens.
111 Together these analyses identify genes and pathways essential in the HS-response,
112 implicating oxidative stress and protein-damage responses, host-cell remodelling, and
113 unexpectedly, apicoplast isoprenoid biosynthesis. Apicoplast-associated genes in
114 general were up-regulated in response to HS, as were other *Plasmodium* genes with
115 orthologs in plant and algal genomes. Finally, parallel phenotyping of a mutant library
116 revealed a significant overlap between parasite pathways underlying the response to
117 febrile temperatures and those implicated in the artemisinin mechanism of action (MOA),
118 including oxidative stress, protein-damage responses, and apicoplast-mediated vesicular
119 trafficking [7, 8]. Mutants in known protein-targets of artemisinin tended to be sensitive to
120 HS [9], and expression-data from recent field-isolates directly correlates artemisinin-
121 resistance with HS tolerance in our pooled screen [10]. Further, we found the K13-
122 associated parasite endocytosis pathway responsible linked to artemisinins resistance
123 [11, 12] is also downregulated in response to HS. Together these data identify an
124 unexpected link between artemisinin MOA, HS-survival, and algal origins of the
125 apicoplast, suggesting the parasite exploits its innate fever-response mechanisms to
126 gain resistance to artemisinin. This study creates a blueprint for developing a large-scale
127 phenotypic screening pipeline of the *P. falciparum pB*-mutant library to enable high-
128 throughput interrogation of phenotypes of interest to hasten further biological insight that
129 can be weaponized against the parasite.

130

131 **RESULTS**

132 **Pooled screens of an extensively characterized pB-mutant clone-library allow**

133 **robust identification of heat-shock phenotypes**

134 To interrogate pathways and processes associated with parasite survival at febrile

135 temperatures, we developed a large-scale phenotypic screening pipeline to analyze the

136 phenotypes in pooled *pB*-mutant parasites exposed to HS-induced stress (Fig. S1). We

137 previously demonstrated using individual clonal *pB*-mutant parasite lines that mutant

138 growth-phenotypes can be detected and differentiated in pooled screening utilizing

139 QIseq—"Sensitive" mutants with disruptions in genes/genomic features important for

140 growth have lower QIseq reads, while "Neutral" disruptions in features not vital for

141 growth under the same conditions have higher reads [13]. We therefore reasoned that

142 mutants with mutations in genes underlying the HS-response would grow poorly in

143 response to HS compared to mutants in genes not contributing to HS-survival.

144

145 We used a pool of 128 unique, extensively characterized *P. falciparum pB*-mutant clones

146 reflecting disruptions in genes spanning a range of functional categories, as well as

147 many genes without existing functional information, as a "pilot library" for initial

148 phenotypic screen-development ([13, 14]; Methods). An *in vitro* HS-screen of this pilot-

149 library, adapted from a phenotype- screen of many *pB*-mutant-clones comprising the

150 pilot-library [15], defined *pB*-mutant HS-response phenotypes to fever-like temperatures

151 (Fig. 1A-E, Table S1, Methods). We next calculated a measure of fitness for each

152 mutant in response to HS while also taking into account inherent differences in mutant-

153 growth in ideal conditions, which we termed the Phenotypic-Fitness Score in response to

154 HS (PFS_{HS}; Methods). We classified 28 mutants of the pilot-library as HS-Sensitive (Fig.

155 1E-F, indicated in red; Table S1). Fourteen mutants performed poorly in both the

156 Growth- and HS-Screens (Fig. 1E-F, yellow). We classified 28 mutants displaying a
157 slight growth advantage in response to HS (Fig. 1E-F, green) as “HS-Tolerant”. Mutants
158 exhibiting neither sensitivity nor tolerance to HS were classified as HS-Neutral (n = 49).
159
160 QIseq-data resulting from the HS- and Growth-screens allowed robust assignment of
161 mutant-phenotypes for both (see Methods). We primarily classified mutants sensitive to
162 heat-shock alone as HS-Sensitive to avoid possible over-interpretation of generally-sick
163 Growth-Sensitive mutants (Fig. 1E-G).
164
165 **Pooled phenotypic screens scaled up to a 1K *pB*-mutant library enable**
166 **identification of processes driving the *P. falciparum* heat-shock response**
167 We next scaled our pooled HS-screen to a mutant library of 922 functionally
168 uncharacterized mutants using the methods we established in our pilot-library screens.
169 This 1K-library comprised mutant-pools randomly selected from our saturation library,
170 covering genes annotated to diverse GO-categories, as well as many genes of unknown
171 function. Mutants were ranked by fold-change growth in response to HS from HS-
172 Sensitive to HS-Tolerant, as per cut-offs determined from our pilot-library screens. Our
173 analysis distinguished 149 mutants growing well in ideal growth conditions but poorly in
174 response to HS as HS-Sensitive (FC-HS < 0.5 and PFS_{HS} < 0.25; Fig. 2A, red box),
175 while 91 mutants performed poorly in both the Growth- and HS-screens (FC-HS < 0.5
176 and PFS_{HS} > 0.25; yellow). Of the remaining mutants, 139 HS-Tolerant mutants had
177 slightly better growth in HS than ideal growth-conditions (FC-HS > 1.5; green box), while
178 543 classified as HS-Neutral were neither sensitive nor tolerant (taupe).
179
180 This larger scale of screening allowed us to assess gene functional-enrichment in HS-
181 Sensitive and Growth-Sensitive phenotypic categories vs all other mutants in the ~1K-

182 library. HS-Sensitive mutants were enriched in GO terms associated with HS-response
183 such as protein-folding, response to DNA-damage, DNA-repair, and regulation of
184 vesicle-mediated transport, broadly in agreement with processes identified to underlie
185 the HS-response by more conventional gene expression-based methods [4, 5]. Growth-
186 Sensitive mutants tended to be enriched for more general categories broadly important
187 for survival in all conditions, such as translation- or mRNA-metabolism-related terms
188 (Fig. 2B), as might be expected given the high essentiality of these processes in ideal
189 growth [6, 16].

190 **Increased transcription of the unfolded protein response (UPR), organelle-**
191 **targeted stress-response pathways and host-cell remodeling characterize the**
192 **parasite HS-response**

193 We characterized the wildtype parent-NF54 transcriptome in response to HS to establish
194 a baseline for comparison using an experimental design similar to a prior study to
195 assessing transcriptional changes in response to febrile temperatures via microarray [5].
196 The HS assay-design mimicking parasite exposure to malarial fever was modelled after
197 conditions we established for our pooled-screens (Methods). RNAseq was performed on
198 heat-shocked parasites vs. a non-heat-shocked control. Genes identified as differentially
199 expressed in response to febrile temperatures vs. 37°C were classified into three
200 different categories based on direction of response: (1) upregulated in response to HS;
201 (2) downregulated in HS, and (3) neutral in HS (Fig. 3A-B, Table S3A). The majority of
202 genes expressed above threshold in our analysis were HS-neutral (1541 genes out of
203 2567, or ~60%) and were enriched for genes involved in general housekeeping functions
204 such as the proteasome core complex (ubiquitin-proteasome system), the ubiquitin-
205 dependent ERAD-pathway, and regulators thereof), RNA metabolism (RNA-binding,
206 mRNA-splicing) and transport functions (e.g. protein import into nucleus, vesicle-

207 mediated transport). We primarily considered genes upregulated in HS as drivers of the
208 HS-response.
209
210 Genes upregulated in HS (n = 415) tended to be enriched for processes such as protein-
211 folding, unfolded protein-binding, response to heat, mitochondrial processes, and host-
212 cell remodelling-associated exported proteins localizing to the Maurer's clefts (Fig. 3B,
213 Table S3C-D). Genes downregulated in HS (n = 611) tended to be enriched for
214 pathogenesis-related functions and components of the parasite invasion machinery,
215 such as entry/exit from the host cell and cell-cell adhesion, and organelles including the
216 inner-membrane pellicle complex, micronemes, and rhoptries. These data are in general
217 agreement with previously-reported processes expected to drive the parasite HS-
218 response [4, 5].
219
220 **The unfolded protein response, organelle-targeted pathways are dysregulated in**
221 **HS-Sensitive mutants**
222 We reasoned that genes dysregulated in HS-Sensitive mutants compared to wildtype
223 underlie the HS-response. We chose two individual HS-Sensitive mutant clones for
224 additional profiling via RNAseq to identify dysregulated genes responsible for this
225 sensitivity. Both mutant lines have a single disruption in the coding region of a gene not
226 previously implicated in the HS-response: *ΔDHC* (dynein heavy-chain gene
227 PF3D7_1122900), and *ΔLRR5* (leucine-rich repeat protein PF3D7_1432400).
228
229 The 1298 genes which could be classified into HS-response categories across all three
230 parasites were analyzed for functional-enrichment (Table S3B). The majority of genes
231 were HS-neutral across all three parasites and were enriched for essential
232 housekeeping functions (n = 615; Table S3B-D). We reasoned these non-HS-regulated

233 genes have functions too important for basic survival to tolerate large stress-associated
234 expression-changes, and these genes were not considered drivers of the HS-response.
235 We identified 91 genes significantly upregulated in HS across all three parasites, which
236 were functionally enriched for protein-folding, chaperone-related processes, and other
237 processes related to heat-stress and the UPR, in agreement with previous expression-
238 based studies [5], as well as enrichment-results from HS-Sensitive mutants in our pooled
239 screening, indicating the parasite increases production of heat-shock proteins (HSPs)
240 and associated chaperones to repair the glut of proteins damaged/misfolded by heat-
241 stress (Table S3B-D). Energy-producing processes (gluconeogenesis, glycolysis) were
242 also upregulated, suggesting the parasite reroutes anabolic metabolism to increase
243 energy production to support ATP-dependent processes such as protein-refolding to
244 correct heat-damaged proteins. Genes upregulated in HS were further enriched for
245 processes involved in host-cell remodeling, including genes targeted to the Maurer's
246 clefts, the host cell, and intracellular vesicles—all known to be important for parasite-
247 remodeling of the host-cell to promote structural reinforcement against heat-shock
248 damage to ensure its own survival [4, 5]. Organellar targeting to the mitochondria and
249 apicoplast are also enriched in upregulated HS-responsive genes. The parasite's
250 increased utilization of mitochondrial stress-response pathways may aid in degrading
251 heat-damaged proteins that cannot be correctly refolded. Increased activity in the food
252 digestive vacuole may allow the parasite to phagocytose and eliminate toxic misfolded
253 protein-aggregates. The apicoplast involvement, particularly the isoprenoid biosynthesis
254 pathway, has not been previously implicated in the HS-response.
255
256 Genes downregulated in all three parasites in response to HS (n = 205) were enriched
257 for virulence-factor and invasion-machinery-associated GO terms, suggesting the

258 parasite decreases production of transcripts associated with pathogenesis, invasion and
259 egress, lengthening its intracellular recovery-time to address global protein-damage.
260
261 Both HS-Sensitive mutants share many characteristic features of the wildtype response
262 to febrile temperatures, which likely enabled their survival (Fig. 3A-B, red, blue; Table
263 S3C-D). We identified two primary expression categories of genes dysregulated in the
264 HS-Senstive mutants: (1) genes upregulated in the wildtype HS-response that were
265 otherwise dysregulated in the HS-Sensitive mutants, which we interpreted as loss-of-
266 function changes, and (2) genes that were not regulated in response to HS in the
267 wildtype but were upregulated in the HS-Sensitive mutants, presumably equivalent to
268 dominant-negative gain-of-function changes (Fig. 3A-B, ochre and tan, respectively).
269 This first category of mutant-dysregulated genes was enriched for the UPR, as well as
270 mitochondrial and apicoplast-localized pathways (cytochrome oxidase-assembly and
271 fatty-acid biosynthesis, respectively). Several apicoplast isoprenoid biosynthesis-related
272 genes upregulated in the wildtype HS-response were additionally dysregulated in one or
273 both HS-Sensitive *pB*-mutant clones (Fig. 3C). The second category of mutant-
274 dysregulated genes, those that are not HS-responsive in wildtype, were enriched for
275 translation-associated processes.
276
277 These data taken together suggest underlying mechanisms responsible for the HS-
278 response. Critically, HS-Sensitive mutants fail to upregulate mitochondrial and apicoplast
279 stress-response pathways, as well as signal peptide-processing pathways that might
280 enable appropriate activation of those pathways. Mutants do not increase production of
281 transcripts associated with responding to unfolded proteins. HS-Sensitive mutants
282 additionally upregulate translation-related processes in response to HS when translation
283 should be paused or neutral. This increase may overwhelm the parasite's capacity to

284 repair or degrade heat-damaged proteins, exacerbating the formation/accumulation of
285 toxic misfolded-protein aggregates that increase parasite sensitivity to HS.
286
287 **Apicoplast isoprenoid biosynthesis is critical for *P. falciparum* survival of febrile**
288 **temperatures**
289 We examined our RNAseq data more closely to discern contributions of the apicoplast to
290 HS-survival. We found that apicoplast-targeted genes tended to be increased in
291 response to HS as compared to all non-apicoplast-targeted genes (Fig. 4A), were more
292 likely to be essential during ideal blood-stage growth conditions (Fig. 4B), and were
293 enriched for stress-response processes such as the UPR and oxidative-stress, and less
294 expectedly, isoprenoid biosynthesis (Fig. 4C). As a major function of isoprenoid
295 biosynthesis is in protein-prenylation—an important post-translational modification that
296 regulates protein-targeting and function throughout the cell—we hypothesized that
297 mutants in known-prenylated proteins [17, 18] would also have a phenotype in HS. We
298 examined our 1K mutant-library for representation of isoprenoid biosynthesis, its
299 immediate upstream-regulators (proteins responsible for modulation and import of
300 glycolytic intermediates that serve as pathway substrates), and immediate downstream-
301 effector proteins, and found that all eight isoprenoid biosynthesis-related *pB*-mutants
302 included in the pooled screen were indeed HS-Sensitive (Fig. 4D).
303
304 Based on these data we further hypothesized that proteins or pathways allowing *P.*
305 *falciparum* survival of febrile temperatures would be absent or otherwise divergent in
306 *Plasmodium* species whose hosts do not mount fever-responses. We therefore
307 compared the apicoplast isoprenoid biosynthesis pathway between *P. falciparum* and
308 two rodent-infective species, *P. berghei* and *P. yoelii*. We found key thiamine-synthesis
309 enzymes directly upstream of the pathway missing in the rodent-infective malaria

310 parasites, including hydroxy-ethylthiazole kinase (ThzK); ThzK is up-regulated in the
311 canonical parasite response to febrile temperatures and dysregulated in HS-Sensitive
312 mutants (Fig. 4E). Perhaps most importantly, DOXP-Synthase (DXS), the critical
313 enzyme marking the first step in isoprenoid biosynthesis, is upregulated in HS,
314 dysregulated in HS-Sensitive mutants, and was HS-Sensitive in pooled screening, as
315 were all four members of the prenylated blood-stage proteome represented in our
316 screen (Fig. 4E). These data taken together strongly implicate isoprenoid biosynthesis in
317 the HS-response.
318
319 Though the apicoplast has not previously been implicated in parasite survival of febrile
320 temperatures, there is extensive literature on the ability of plants to mount effective
321 defenses against heat as well as other external stressors, particularly critical for non-
322 motile organisms at the mercy of their environments. We investigated the relationship
323 between the parasite's HS-response and "plant-like" stress-responses by evaluating
324 phyletic distribution of parasite HS-response genes in representative plant and algal
325 genomes. *P. falciparum* genes with plant orthologs indicating potential endosymbiont-
326 ancestry tended to be increased in response to HS vs. genes that do not have plant
327 orthologs (Fig. 4F). These lines of evidence considered together present an evolutionary
328 explanation that endosymbiosis of the apicoplast's algal progenitor enabled parasite-
329 survival of extreme temperatures.
330
331 **Processes enabling parasites to survive fever also drive resistance to artemisinin**
332 We noted similarities between processes we identified to be driving the parasite HS-
333 response and those implicated in parasite-resistance to artemisinin [7, 8, 10]. Therefore,
334 we did a series of parallel phenotype- screens of our *pB*-mutant pilot-library using
335 sublethal concentrations of two artemisinin compounds (dihydroartemisinin, DHA;

336 artesunate, AS), heightened conditions of oxidative stress of RBCs, and exposure to a
337 proteasome inhibitor (Bortezomib; BTZ) to investigate the possible relationship between
338 HS-response and artemisinin MOA. HS-Sensitive mutants tended to be sensitive to both
339 artemisinin derivatives and H_2O_2-induced oxidative stress, while HS-Tolerant mutants
340 were less sensitive to either condition (Fig. 5A, Table S4). Also, HS-Sensitive mutants
341 shared an increased sensitivity to the proteasome inhibitor BTZ, consistent with
342 laboratory observations connecting artemisinin MOA to the proteasome and clinical data
343 that proteasome-inhibitors act synergistically with artemisinins [8, 19-21]. Overall,
344 correlation of mutant phenotypic profiles across screens varied, with 16-45% having
345 correlating phenotypes in at least one additional screen (Fig. 5B, Fig S2A-B).
346
347 We next assessed whether these laboratory-based experimental findings corresponded
348 to 'real world' changes associated with *P. falciparum* in artemisinin-resistant (ART-R)
349 clinical isolates [10]. Consistent with our laboratory findings linking HS- sensitivity and
350 ART- sensitivity, the genes associated with the HS-Sensitive mutants were significantly
351 correlated with genes linked to ART-R in recent field isolates (Fig. 5C, Table S4). We
352 also found clear GO relationships between HS phenotype-categories and ART-R in field-
353 isolates, with genes driving the HS-response most positively correlated with reduced
354 parasite clearance-rates (Fig. 5D, Table S4).
355
356 Artemisinin is activated by degradation of host hemoglobin. Recent evidence has
357 suggested two key, temporally-distinct ART-R mechanisms: (1) a multi-functional protein
358 long associated with resistance in field-isolates, *kelch13* (K13) confers resistance
359 upstream of hemoglobin degradation by modulating an associated endocytosis pathway;
360 and (2) downstream of hemoglobin degradation through the ubiquitin-proteasome
361 system (UPS), where K13 may function as or regulate a ubiquitin ligase [10-12, 22-25].

362 In upstream-resistance, endocytotic transport of hemoglobin to the digestive vacuole
363 (DV) is down-regulated as this is the key process through which the parasite ingests,
364 degrades, and then releases hemoglobin. K13 mutant-isolates appear to downregulate
365 processes along this endocytosis pathway, decreasing parasite hemoglobin digestion
366 and release of heme to activate artemisinin, thereby increasing parasite survival (Fig.
367 S2C). We found that K13-defined endocytosis is also downregulated in response to HS
368 (Fig. 5E). As the K13-mediated endocytosis pathway culminates in host haemoglobin-
369 cargo being degraded in the DV, we further assessed our 1k HS-screen for DV-
370 associated proteins. We found DV-associated proteins did tend to be sensitive to heat-
371 shock, including key DV resident-proteases (Plasmepsin I, M1-family alanyl
372 aminopeptidase; Fig. S3A) [26]. We next evaluated our 1K HS-sScreen for direct K13-
373 interacting partner-proteins recently identified via immunoprecipitation [25], and found
374 that mutants in 10 of the 24 unique putative K13-partner-proteins represented in the
375 screen were sensitive to HS. Further, 5 of 7 known alkylation-targets of artemisinin
376 represented in our screen had sensitivity to HS [9, 26] (Fig. S3B). We noted significant
377 overlap in each of these categories of ART MOA-related genes and isoprenoid
378 biosynthesis-related genes (Fig. S3C).
379
380 In a second downstream step post-activation of artemisinin, the parasite engages the
381 UPS to further mitigate artemisinin-induced damage. Artemisinins mount a multi-pronged
382 attack against the parasite by causing a global, non-specific accumulation of damaged
383 parasite proteins, which are then polyubiquitinated/marked for degradation, while also
384 inhibiting proteasome-function. These poly-ubiquitinated proteins ultimately overwhelm
385 the parasite's decreased capacity for UPS-mediated protein-degradation [8]. Key
386 ubiquitinating components of this system, including E2/E3 ligases and K13, are
387 downregulated in response to HS, while key components of the UPR and protein folding

388 are increased (Fig. 5E). In contrast, components of the core proteasome were
389 universally increased in response to HS when considered in aggregate, although the
390 change did not meet our fold-change criteria for being HS-regulated (Fig. S4).
391
392 Synthesizing these data, we present a model for the relationship between DHA MOA
393 described recently [8] and HS-response (Fig. 5F). The canonical parasite-response to
394 fever is to increase protein-folding and UPR while inhibiting ubiquitination to prevent
395 accumulation of toxic, polyubiquitinated protein-aggregates. The parasite simultaneously
396 increases its capacity for proteasome-mediated degradation—ultimately enabling it to
397 resolve HS-instigated stress and thus survive febrile temperatures. Artemisinins kill by
398 overwhelming these same pathways: damaging and unfolding proteins, preventing
399 folding of newly synthesized proteins and inhibiting the proteasome, while at the same
400 time activating ubiquitination-machinery to ensure the accumulation of toxic
401 polyubiquitinated proteins that eventually cause cell-death. ART-R-associated mutations
402 allow the parasite to constitutively activate unfolded-protein response mechanisms which
403 increase its capacity for refolding or degrading those toxic proteins [27]. The overall
404 increase in damaged-protein degradation-capacity allows ART-R parasites to keep up
405 with the influx of artemisinin-induced protein-damage, clearing the waste and enabling
406 parasite survival. This direct inverse relationship in activation of endocytosis, the
407 ubiquitin-proteasome system and other pathways underlying DHA-mediated killing and
408 febrile-temperature survival, supports a shared mechanism for artemisinin-resistance
409 and HS-response, suggesting that ART-R parasites evolved to harness canonical HS-
410 survival mechanisms to survive artemisinin.
411
412 **Discussion**

413 Our data indicate that the parasite crisis-response to HS is multi-faceted to relieve the
414 build-up of heat-damaged proteins before it is overwhelmed by toxic, misfolded-protein
415 aggregates. Responding to or perhaps preventing a build-up of potentially toxic heat-
416 damaged proteins, the parasite upregulates expression of chaperones to stabilize and
417 detoxify them, downregulating ubiquitinating enzymes to discourage their aggregation
418 while upregulating the core proteasome and vesicular trafficking to degrade and
419 eliminate proteins which can't be repaired. Equally important in the survival-response are
420 changes in redox homeostasis, lipid metabolism, cellular transport, and metabolic
421 processes associated with the endosymbiont-derived organelles. The parasite requires
422 increased energy to mount this febrile response, which it provides by redirecting its own
423 internal biosynthetic pathways to produce glucose. Interestingly, we confirm the
424 parasite's protective response-mechanisms include proteins exported into the
425 erythrocyte, suggesting that the parasite's metabolic processes exported to remodelled
426 cytoplasm of the parasitized host cell are equally vulnerable and vital to malaria parasite
427 survival.
428
429 A high proportion of essential genes that are upregulated in response to heat stress are
430 targeted to the apicoplast. The apicoplast isoprenoid biosynthesis pathway's critical
431 involvement in survival of febrile temperatures is nevertheless a surprise, as it has not
432 been implicated before in the *Plasmodium* HS-response. Isoprenoids are required for
433 myriad functions across the tree of life—plant chloroplasts, algae, some parasitic-
434 protozoa and bacterial pathogens utilize a specialized form of this pathway absent from
435 all metazoans (called the non-mevalonate, MEP, or DOXP pathway), which has made
436 isoprenoid biosynthesis an attractive target for intervention against a range of pathogens
437 [28, 29]. Most studied organisms make wide use of protein-prenylation and have large
438 prenylated proteomes; malaria parasites, in contrast, have a very small prenylated

439 blood-stage proteome (~20 proteins) consisting primarily of vesicular trafficking proteins,
440 notably the Rab-family GTPases [17, 18]. Recent studies indicate the key essential
441 function of isoprenoids in the parasite blood-stage is in their roles as substrate for
442 protein-prenylation—specifically, in prenylating proteins driving vesicular transport to the
443 digestive vacuole [30, 31]. In the absence of prenylation, Rab5 trafficking is disrupted,
444 which leads to digestive vacuole-destabilization and parasite death [31]. Notably,
445 artemisinin also disrupts digestive vacuole-morphology, resulting in a very similar
446 phenotype as a consequence of its activation via hemoglobin digestion [32, 33].
447 Intriguingly, recent data confirm the association of key resistance-mediator K13 with
448 Rab-GTPases [25], adding to the repertoire of proteins comprising K13-mediated
449 endocytic vesicles, and by extension supporting the role of prenylation in K13-mediated
450 processes associated with ART MOA.
451
452 Another key parasite-defense against oxidative stress induced by pro-oxidant
453 compounds (such as artemisinin) includes increased vitamin E biosynthesis—another
454 exclusive function of the MEP isoprenoid-biosynthesis pathway, whose stress-related
455 regulation has been extensively studied in plants [34, 35]. Further insights to the role
456 isoprenoids play in the HS-response may be gleaned from plants and pathogenic
457 bacteria, where research suggests key branchpoint-enzyme DXS, which catalyzes the
458 first and rate-determining step of the MEP pathway [36], has a role in sensing and then
459 facilitating adaptation to ever-changing environmental conditions, including temperature,
460 light-exposure, chemical compounds, and oxidative stress (for example [37, 38]).
461 Elevated levels of isoprenoids have been found to correlate with plant exposure to
462 drought and other stressors and are considered a key component of plant-defenses
463 against abiotic stress [39]. The DXS ortholog may play a similar role in *P. falciparum*,

464 enabling the parasite to mount quick responses to unfavorable conditions in the host-
465 environment, such as fever.
466
467 Interestingly, concurrent studies now provide mechanistic insights illuminating the
468 biochemical relationship between apicoplast isoprenoid biosynthesis and the parasite
469 febrile-temperature survival response (co-submission by Mathews et al.). Farnesylation
470 of HSP40 (PF3D7_1437900), a type of prenylation mediated by the MEP pathway, is
471 critical for *P. falciparum* survival of thermal stress. In this study Inhibition of isoprenoid
472 biosynthesis ultimately resulted in reduced association of HSP40 with critical
473 components of the cytoskeleton, protein-export, and vesicular transport pathways—
474 without which *P. falciparum* could survive neither heat nor cold stress. Suppression of
475 these cellular processes by loss of HSP40-farnesylation directly corresponds to HS-
476 sensitive pathways identified via both our forward-genetic screen and our gene-
477 expression analyses of the HS-Sensitive LRR5- and DHC4-mutant clones.
478
479 Few eukaryotes are known to be able to thrive in extreme-heat environments; most are
480 unable to complete their lifecycles above 40°C [40]. The survival mechanism of malaria
481 parasites could be attributed to the algal ancestral lineage of the apicoplast. Some
482 extant red algal-lineages (genus *Cyanidioschyzon*) are extremophilic inhabitants of
483 acidic hot-springs and are remarkably resistant to heat shock up to 63°C; green-algae
484 *Chlamydamonas reinhardtii* was also able to survive to 42°C [41]. Responsibility for this
485 extreme resistance to transient exposure to high temperatures was attributed to two
486 genes of the small heat shock protein (sHSP) family (CMJ100C and CMJ101C). The *P.*
487 *falciparum* ortholog for these genes (PF3D7_1304500) was upregulated in the wildtype
488 HS-response and dysregulated in both our HS-Sensitive mutants, indicating its

489 contribution to parasite survival in extreme temperatures. Mutations in this gene were
490 not represented in our pooled screens.
491
492 It is tempting to speculate that acquisition of the red-algal endosymbiont and its
493 associated plant stress-response mechanisms is what enabled the ancestral parasite to
494 survive host-fever, likely an important and early step leading to successful infection of
495 hominid hosts. Our findings of significant overlap between parasite-responses to three
496 disparate stressors (HS, artemisinin, oxidative stress) offers new insight into how *P.*
497 *falciparum* exhibited artemisinin-resistance even in the initial clinical trials [42], and then
498 further evolved resistance relatively quickly after mass-introduction of the drug by
499 “hijacking” and repurposing the parasite's in-built fever-response pathways.
500
501 **Conclusion**
502 Deeper knowledge of parasite biology is expected to enable more effective and likely
503 longer-lasting antimalarial interventions. Similarly, a better mechanistic understanding of
504 artemisinin MOA will lead to better combination therapies to combat emerging
505 resistance. With this first large-scale forward-genetic screen in *P. falciparum*, we
506 revealed the parasite’s survival responses to malarial fever and artemisinin
507 chemotherapy share common underpinnings that heavily depend on metabolic
508 processes of plant origin.
509
510 ART-R ultimately hinges on highly efficient protein-degradation mechanisms. This
511 mechanistic knowledge allows for the application of intelligently considered counters to
512 ART-R, such as combinatorial therapy with proteasome-inhibitors, which has
513 experimentally shown great promise [43]. Our current study highlights the potential of
514 forward-genetic screens to elucidate unexpected processes and pathways, such as

515 DOXP and isoprenoid biosynthesis, that are associated with the artemisinin MOA which
516 may serve as synergistic druggable targets. Future studies can exploit a genome-wide
517 screening approach to iteratively ascribe function to every part of the malaria-parasite
518 genome to support targeted development of new, more-efficacious antimalarial
519 combination therapies to limit and potentially reverse artemisinin resistance.
520

521 **Declarations**

522 *Ethics approval and consent to participate*

523 Not applicable.
524

525 *Consent for publication*

526 Not applicable.

527 *Availability of data and materials*

528 The raw RNAseq dataset supporting the conclusions of this article are available in the
529 Mendeley Data repository *Malaria-parasite survival of host fever is linked to artemisinin*
530 *resistance*, http://dx.doi.org/10.17632/b8g3wbnd5v.1 [44]. Raw QIseq dataset accession
531 numbers are listed in Table S5.
532

533 *Competing interests*

534 The authors declare that they have no competing interests.
535

536 *Funding*

537 This work was supported by the National Institutes of Health grant R01 AI094973 and
538 R01 AI117017 (J.H.A.) and the Wellcome Trust grant 098051 (J.C.R.).
539

540 *Authors' contributions*

541 Conceptualization, M.Z., C.W., J.O., T.D.O., J.C.R., M.T.F., R.H.Y.J., and J.H.A.;
542 Methodology, M.Z., C.W., J.O., K.B.S., R.H.Y.J., and J.H.A.; Software, J.O. and C.W.;
543 Validation, M.Z., C.W., and J.O.; Formal Analysis, M.Z., C.W., J.O., S.R.A., and
544 R.H.Y.J.; Investigation, M.Z., C.W., J.O., P.T., D.C., S.B., S.X., M.M., and R.H.Y.J.; Data
545 Curation, M.Z., C.W., and J.O.; Writing—Original Draft, J.O., M.Z., and J.H.A.; Writing—
546 Review & Editing, J.O., M.Z., T.D.O., J.C.R. and J.H.A.; Visualization, C.W., M.Z., J.O.,
547 and R.H.Y.J.; Supervision, M.Z., J.O., T.D.O., J.C.R., M.T.F., R.H.Y.J., and J.H.A.;
548 Project Administration, M.Z.; Funding Acquisition, J.C.R. and J.H.A.
549

550 *Acknowledgements*

551 We appreciate the Wellcome Sanger Institute (United Kingdom) for performing QIseq
552 and Xiangyun Liao, Suzanne Li, and Kenneth Udenze for support of parasite cell culture.
553 We thank the USF Genomics Program Omics Hub for productive discussion.
554

555 **FIGURE LEGENDS**

556 **Figure 1. Pooled screens of *P. falciparum piggyBac* mutants allow robust**
557 **identification of heat-shock phenotypes. A.** Experimental design for pooled heat
558 shock (HS) phenotypic screens. The pilot library of *pB*-mutant clones (n=128) was
559 exposed to three rounds of temperature-cycling to simulate malarial fever (Methods). A
560 pilot-library control concurrently grown continuously at 37°C established inherent growth
561 of each *pB* mutant.
562 **B.** QIseq quantifies each *pB*-mutant in the pilot library from sequence-reads of the 5′ and
563 3′ ends of each *pB* insertion-site. Colored lines represent genes. Black boxes indicate
564 transposon location.

565 **C.** Pilot-library mutant growth-phenotypes at ideal temperatures, defined as fold change
566 in QIseq reads-count after three cycles growth at 37°C (FC-Growth; Methods) ranked
567 from Sensitive to Tolerant. Mutants with inherently slower or faster growth under ideal
568 conditions are shown in grey and blue, respectively.
569 **D.** Pilot-library mutant HS-phenotypes ordered from Sensitive (red) to Tolerant (green).
570 Mutant growth was defined as QIseq reads-count fold-change in response to HS (FC-
571 HS) vs. non heat-shocked control (Methods). HS-Sensitive mutants have lower FC-HS
572 (red, FC-HS < 1), while HS-Tolerant mutants have higher FC-HS (green, FC-HS > 1).
573 **E-F.** HS- and Growth-phenotypes of the pilot-library mutants. HS-phenotype of each
574 mutant (displayed as line-graph) is superimposed on its corresponding Growth-
575 phenotype (bar graph). Red = HS-Sensitive mutants (FC-HS < 0.5 and Phenotypic
576 Fitness Score in response to heat shock (PFS_{HS}) < 0.25, n = 28). Yellow = mutants
577 classified as both Growth-Sensitive and HS-Sensitive (FC-HS < 0.5, PFS_{HS} > 0.25, n =
578 14). Green = HS-Tolerant mutants (FC-HS > 1.5, n = 30). Mutants neither Sensitive nor
579 Tolerant to HS were classified as HS-Neutral (n = 49). *Known HS-Sensitive *pB*-mutant
580 clones validated by individual HS-assay [15]. **Known HS-Tolerant *pB*-mutant clones
581 validated by individual HS-assay [15].
582 **G.** Distributions of PFS_{HS} for mutant HS-phenotype classifications. HS-Sensitive mutants
583 are assigned the lowest PFS_{HS}, while HS-Tolerant mutations are assigned the highest
584 PFS_{HS} (**** Wilcoxon-test p-value < 1e-15) (Methods).
585
586 **Figure 2. Large-scale pooled phenotypic screens enable identification of**
587 **processes driving the *P. falciparum* heat-shock response**
588 **A.** HS-Sensitive mutations identified in pooled screens of 922 *pB*-mutants. Mutant pools
589 were screened in both ideal growth conditions and under HS and were assigned
590 phenotypes as per methods established in the pilot-library screens (Fig. 1). Mutants are

591 ranked by fold-change in response to HS (FC-HS; n = 922) from HS-Sensitive (red; n =
592 149) to HS-Tolerant (green; n = 139). Mean mutant fold-change in ideal growth (FC-
593 Growth) is superimposed as a bar plot (gray, FC-Growth < 1.0; blue, FC-Growth > 1.0).
594 Mutants performing poorly in both screens (yellow; n = 91) were classified as HS- and
595 Growth-Sensitive and were not considered further. Mutations neither HS-Sensitive nor
596 HS-Tolerant were classified as HS-Neutral. See Methods and Table S2.
597 **B.** Functional enrichment of GO terms for HS-Sensitive or Growth-Sensitive *pB*-mutants
598 vs all other mutants in the 1K-library. HS-Sensitive mutants were enriched in terms
599 associated with HS-response such as protein-folding, response to DNA-damage, DNA-
600 repair, and regulation of vesicle-mediated transport. Growth-Sensitive mutants tended to
601 be enriched for more general categories broadly important for survival in all conditions,
602 such as translation- or mRNA-metabolism-related terms. Circles represent GO category,
603 circle color represents ontology, and circle size represents number of significant genes
604 annotated to that category. Significant terms (Fisher/elim-hybrid test p. value <= 0.05)
605 fall within the light-green box.
606
607 **Figure 3. Increased transcription of the unfolded protein response, organelle-**
608 **targeted stress-response pathways and host-cell remodeling characterize the**
609 **parasite HS-response. A.** Genes were classified based on their NF54-expression with
610 and without HS-exposure across all three parasite lines (Methods). Genes were
611 classified as upregulated in response to HS (FC-HS > 1; ↑), down-regulated in response
612 to HS (FC-HS < -0.5; ↓), or not regulated by HS (-0.5 < FC-HS < 1; –), with upregulated
613 genes considered to be driving the HS-response. Genes were then assigned HS
614 expression-categories based on phenotype in NF54 vs. HS-Sensitive mutants *ΔLRR5*
615 and *ΔDHC*. HS-regulated genes shared between NF54 and both mutants are indicated
616 in red (↑↑↑) or blue (↓↓↓) for up- and down-regulated genes, respectively. Genes

617 dysregulated in one or both HS-Sensitive mutants fell into two main expression-profile
618 categories underlying mutant HS-Sensitivity phenotypes: those upregulated in NF54 that
619 failed to be regulated in the mutants (↑⤱⤱), and genes not regulated in response to HS
620 in NF54 that were inappropriately upregulated in the mutants (– ↑↑).
621 **B.** Functional enrichment analyses between wildtype/mutant HS-expression profiles as
622 defined in A. Red: Shared upregulated HS-responsive GO-terms between NF54 and the
623 two HS-Sensitive *pB*-mutants (↑↑↑). Blue: Shared down-regulated HS-responsive GO-
624 terms (↓↓↓). Ochre: GO-terms upregulated in NF54 but dysregulated in the two *pB*-
625 mutant (↑⤱⤱). Tan: GO-terms enriched in genes not regulated in the wildtype HS-
626 response but upregulated in the mutants (– ↑↑). Only enriched GO-terms are shown
627 (Fisher/elim-hybrid test p. value <= 0.05), with highest significance indicated in dark
628 green. Fraction of significant genes mapping to a GO-term in an HS expression-profile
629 category vs. genes mapping to that GO-term in the entire analysis is indicated by
630 distance to the center of the circle, with the outermost position on the circle indicating
631 100% of genes in that GO-term are significant. See Table S3D.
632 **C.** Several apicoplast and isoprenoid biosynthesis-related genes have a tendency to be
633 upregulated in the wildtype-response to HS and are dysregulated in one or both HS-
634 Sensitive *pB*-mutant clones (↑⤱⤱). * Isoprenoid biosynthesis-related genes upregulated
635 by HS confirmed in the pooled HS-Screen.
636
637
638 **Figure 4. Apicoplast isoprenoid biosynthesis is critical for *P. falciparum* survival**
639 **of febrile temperatures. A.** Apicoplast-targeted genes tend to be increased in response
640 to HS as compared to all non apicoplast-targeted genes detected above threshold in
641 RNAseq. Apicoplast-targeted genes are as defined in [45] (*** Fisher-test p-value < 1e-
642 5).

643 **B.** Apicoplast-targeted genes tend to be highly essential during blood-stage vs. all other
644 non-apicoplast-targeted genes detected above threshold in RNAseq. The median
645 Mutagenesis Index Score (MIS; [6]) for apicoplast-targeted genes is much lower than
646 median MIS for all other genes, indicating a lower tolerance for disruption and thus
647 higher likely essentiality during blood-stage development than non-apicoplast-targeted
648 genes (**** Wilcoxon-test p-value < 1e-15).
649 **C.** Apicoplast pathways regulated in response to HS. GO categories enriched in up- and
650 down-regulated apicoplast genes are shown on a scale from red to blue, respectively.
651 The horizontal direction indicates the log ratio between up- and down-regulated
652 apicoplast genes in each category. Circle-size represents gene-number per category.
653 **D.** All nine *pB*-mutants in genes related to apicoplast isoprenoid biosynthesis
654 represented in the 1K-library pooled screen were HS-Sensitive. Mutants are ranked by
655 phenotype from HS-Sensitive (red) to HS-Tolerant (green). Circles indicate each HS-
656 Sensitive mutant related to isoprenoid-biosynthesis. *The three isoprenoid biosynthesis-
657 genes we identified as directly upregulated in response to HS via RNAseq (DXS, tRNA
658 m(1)G methyltransferase and apicoplast RNA methyltransferase). See Table S3.
659 **E.** Key enzymes in the *P. falciparum* isoprenoid biosynthesis-pathway are up-regulated
660 in response to heat-shock (red circle), dysregulated in HS-Sensitive mutants (ochre) and
661 absent in malaria-parasites of hosts that do not present fever. Pathway diagram
662 modeled from [46]. Isoprenoid biosynthesis-genes upregulated in HS include DXS, 1-
663 deoxy-D-xylulose-5-phosphate synthase (DOXP), 2-C-methyl-D-erythritol 2,4-
664 cyclodiphosphate synthase (IspF), pyruvate kinase II (PyKII), triosephosphate isomerase
665 (TIM), triose phosphate transporter (TPT), and upstream-regulator of MEP-pathway
666 substrates HAD1-phosphotase [47]. All vesicular trafficking-proteins RAB GTP'ases,
667 direct downstream-targets prenylated by the MEP-pathway (zigzag) represented in
668 pooled screening were HS-Sensitive. The key thiamin-synthesis enzyme

669 hydroxyethylthiazole kinase (ThzK) is absent in *P. berghei* and *P. yoelii*, malaria-
670 parasites whose rodent-hosts do not present fever.
671 **F**. *P. falciparum* genes with plant orthologs (green circles) indicating potential
672 endosymbiont-ancestry tend to be increased in response to HS vs. genes that do not
673 have plant orthologs (grey circles). *P. falciparum* genes with potential endosymbiont-
674 ancestry were derived from 1919 ortholog-pairs between *Arabidopsis thaliana* and *P.*
675 *falciparum* (data from OrthoMCLv5.0). The listed processes are sorted based on the
676 ratio of "green" to "non-green" orthologs.
677
678 **Figure 5. Increased sensitivity to fever is directly correlated with increased**
679 **sensitivity to artemisinin in the malaria parasite. A.** HS-Sensitive *pB*-mutants (red)
680 are more sensitive to multiple concentrations of artemisinin derivatives Artesunate and
681 Dihydroartemisinin, proteasome-inhibitor Bortezomib (BTZ), and conditions of
682 heightened oxidative stress than HS-tolerant parasites (green) in all pooled screens of
683 the pilot library. *pB*-mutants were cultured continuously under oxidative stress-inducing
684 conditions for three to six cycles (T1 and T2, respectively). Apicoplast-mutants (n = 5)
685 have phenotypes similar to all HS-Sensitive mutants (n =28) in artemisinin-derivative
686 screens, but not to protein-inhibitors or oxidative stress (* Wilcoxon $p < 0.05$; ***
687 Wilcoxon $p < 1e-10$. See Methods).
688 **B.** Correlation between mutant phenotypes in all pooled screens of the pilot library.
689 Mutants performing in the bottom 25% or top 25% of each screen were classified as
690 having "Sensitive" and "Tolerant" phenotypes, respectively. Mutant classifications were
691 compared pair-wise between each screen, with mutants falling into the same category in
692 both screens considered to have correlating phenotypes.
693 **C.** HS-Sensitive *pB*-mutants (red) are positively correlated with genes linked to ART-R in
694 recent field isolates [10](* Wilcoxon test $p < 0.05$).

695 **D.** HS expression-categories as determined by comparative RNAseq between NF54 and
696 two HS-Sensitive mutant clones are positively correlated with ART-R in field-isolates.
697 **E.** Both K13-mediated mechanisms of artemisinin resistance (endocytosis, ubiquitin-
698 proteasome system) are similarly regulated in HS. The K13-defined endocytosis
699 pathway (shades of green) and key ubiquitinating-enzymes of the ubiquitin-proteasome
700 system, E2/E3 and K13, are downregulated in the wildtype NF54 HS-response, while
701 protein folding, stress, exported proteins, and proteasome genes are upregulated.
702 RNAseq data are plotted for each gene by average log2 fold-change in response to
703 HS and significance (–log2(p-value)). Circles in shades of blue and pink indicate genes
704 significantly down- or upregulated after exposure to HS, respectively.
705 **F.** Activation of pathways underlying DHA-mediated killing and febrile-temperature
706 survival is directly inverse. **Top**: Model of DHA-mediated killing in *P. falciparum* adapted
707 from [8]. Artemisinin (ART) damages and unfolds proteins, prevents folding of newly
708 synthesized proteins, and inhibits the proteasome while at the same time activating
709 E1/E2/E3 ubiquitin-machinery. Accumulation of toxic polyubiquitinated protein-substrates
710 (S) overwhelms the cell and leads to death. **Bottom**: Model of parasite fever-response.
711 Heat-stress causes globally damaged protein. The parasite increases the UPR as it
712 inhibits E2/E3 ubiquitination to prevent accumulation of toxic, polyubiquitinated (Ub)
713 protein-aggregates, while at the same time increasing its capacity for proteasome-
714 mediated degradation—ultimately enabling the parasite to resolve HS-instigated stress
715 and survive febrile-temperatures.
716
717 **Methods**
718 *Pilot pB-mutant clone-library characteristics and validation*
719 The single *piggyBac*-transposon insertion sites of each *pB*-mutant-clone in the pilot-
720 library were verified as previously described [13, 14]. Additionally, whole-genome

721 sequencing performed on 23% of 128 *pB*-mutant-clones in the pilot-library verified that
722 no major genomic changes occurred aside from the *piggyBac* insertion, ensuring any
723 detected phenotypes are attributable to the single disruption [15]. The pilot-library was
724 generated in a manner to ensure approximately equal representation of each of the 128
725 clones at thaw [13].
726
727 *Generating the pilot-library of* pB-*mutant parasite clones*
728 The pilot-library was built as described in our previous QIseq methods-development
729 study [13] and data are available in PlasmoDB (RRID:SCR_013331). Aliquots of the
730 pilot-library were generated by first growing each of the 128 extensively-characterized
731 mutant-clones individually in T25-flasks to 1-2% parasitemia. All clones were then
732 combined equally into one large flask and gently mixed. One-hundred equal-volume
733 aliquots of the pilot-library were then cryopreserved according to standard methods.
734
735 *Pooled-screen assay-design*
736 *HS-screens*
737 We exposed pools of *pB*-mutant parasites to three rounds of temperature-cycling to
738 simulate the cyclical pattern of fever characteristic of human malaria (Figure 1A).
739 Parasites under phenotypic selection (heat-shock) and ideal-growth controls originated
740 from the same thaw, grown at 37°C for one cycle then split equally into five flasks (three
741 flasks for exposure to heat-shock, two for the ideal-growth controls). Experimental and
742 control-flasks were maintained in parallel to minimize potential batch-effects. Parasites
743 were grown for one cycle at 37°C until they reached the ring-stage of development
744 (Time-point 0; T^0), at which point the experimental-group were exposed to febrile
745 temperatures (41°C) for 8 hours. Post-heat-shocked parasites were then returned to
746 37°C for the remainder of the 48-hour window until they again reached ring-stage.

747 Parasite-gDNA was harvested for QIseq after two more rounds of temperature-cycling in
748 successive growth cycles to ensure enough parasite-material was available for QIseq
749 (Time-point 1; T^1). Control-parasites were harvested for gDNA before and after three
750 cycles of pooled growth at 37°C (T^0 and T^1, respectively) for quantification via QIseq in
751 technical triplicate. We used QIseq-reads obtained for each mutant after the same
752 number of cycles of pooled growth at 37°C as our T^0 control as previously reported [13].
753
754 *Drug-screens*
755 As with the HS-screen, parasites were split from the same thaw of the pilot-library after
756 one cycle of growth into experimental flasks and control-flasks. Experimental flasks were
757 exposed to three cycles of continuous drug-pressure at two different concentrations
758 (IC10, IC25) of each artemisinin-compound (AS, DHA). Proteasome-inhibitor BTZ-
759 experiments were performed at IC10. Control-flasks were cultured continuously in
760 parallel at 37°C without drug. Parasites were harvested immediately at the conclusion of
761 three growth-cycles for gDNA-extraction and phenotype-analysis via QIseq.
762
763 *Oxidative stress screens*
764 Parasites were split after one cycle of growth from the same thaw of the pilot-library as
765 the HS-screen. Parasites were grown one more cycle, then split into four flasks: two
766 control-flasks to be cultured with standard, washed human red blood-cells (hRBC), and
767 two experimental flasks to be cultured with H_2O_2-treated hRBCs to mimic conditions of
768 oxidative stress. Experimental flasks (H_2O_2 treated-hRBC) and control-flasks (untreated-
769 hRBC) were cultured continuously in parallel at 37°C. Parasites were harvested
770 immediately after three growth-cycles (T1), then again after an additional three growth-
771 cycles (T2) for gDNA-extraction and phenotype-analysis by QIseq.
772

773 Methods for oxidative pre-treatment of hRBCs were as published previously [48]. Briefly,
774 O+ hRBCs (Interstate blood bank, packed, 100% hematocrit) were incubated with 1 mM
775 H_2O_2 (Sigma-aldrich, Cat. no. H1009-100ML) for one hour at room temperature. After
776 treatment, cells were washed three times with phosphate-buffered saline (PBS) before
777 dithiothreitol (DTT) was added to a final concentration of 1 mM to heal any reversible
778 oxidative damages. Cells were then treated with menadione sodium bisulphite for one
779 hour at room temperature (Sigma-aldrich Cat. no. M5750-100G) and washed five times.
780 A volume of 3–4 ml of AB medium (RPMI 1640 medium supplemented with 2 mM L-
781 glutamine, 25 mM HEPES, 100 μM hypoxanthine and 20 μg ml^{-1} gentamicin) was added
782 on top of the cell-pellet after discarding the final wash. Pre-treated erythrocytes were
783 stored at 4 °C before use in parasite culture.
784
785 All pooled screens (HS, AS, DHA, BTZ, oxidative stress, ideal growth) were performed in
786 biological duplicate.
787
788 *QIseq*
789 QIseq, which uses Illumina next-gen sequencing technology and custom library-
790 preparation to enable sequencing from both the 5' and 3' ends of the *piggyBac*
791 transposon out into the disrupted genome-sequence, allows quantitative identification of
792 each *pB*-mutant line by its unique insertion-site within mixed-population pools of *pB*-
793 mutants [13] (Figure 1B). The anatomy of the *piggyBac* transposon and its distinct 5' and
794 3' inverted terminal-repeat sequences (ITRs) allows double-verification of insertion-sites;
795 both 5' and 3' QIseq libraries were therefore generated and sequenced for each sample.
796 Counts per insertion-site were determined as described previously [13]. Measures
797 indicating reproducibility for QIseq-data for both the pilot-library and 1K-library screens
798 are shown in Fig. S5A-B and Fig. S6, respectively. We observed high correlation

799 between 5' and 3' QIseq-libraries from each pool (Fig. S5A, Fig. S6). Resulting Growth
800 and HS phenotype-assignments were highly reproducible across three technical and two
801 biological replicates (HS-Screen, R=0.94; Growth-Screen, R=0.89; Fig. S5B). We found
802 only weak correlation between Growth-Sensitive and HS-Sensitive phenotypes (R =
803 0.44; Fig. S5B, Fig. S6), suggesting that our heat-shock exposure-conditions were
804 sufficient to allow reproducible detection of mutants with specific selection response-
805 phenotypes from pooled screening.
806
807 *Calculating mutant fold-change in pooled screening to assign HS- and Growth-*
808 *phenotypes*
809 We defined FC-Growth by *pB*-mutant fold-change after three cycles of growth at ideal
810 temperatures ($T^{1\text{-}37C}$/ $T^{0\text{-}37C}$). FC-HS was defined as *pB*-mutant fold-change after
811 exposure to heat-shock vs. the non- heat-shocked control ($T^{1\text{-}41C}$/ $T^{1\text{-}37C}$). We used
812 changes in reads-number detected for each *pB*-mutant in the Growth-Screen and the
813 HS-Screen as compared to reads-number detected for that mutant in the respective
814 control-screen to calculate mutant Fold Change (FC) in both screens (Figure 1C-D;
815 Methods). We then ranked mutants from lowest to highest FC, with lowest FC indicating
816 highest sensitivity to the screened-condition.
817
818 We developed a scoring-system to distinguish mutants with phenotypes specifically in
819 the condition under selection (HS) vs. those with inherently compromised growth in ideal
820 conditions, called the Phenotypic Fitness-Score (PFS). PFS_{HS} is the mutant fold-change
821 in response to heat-shock (FC-HS, 41C/37C) multiplied by the ratio of FC-HS to mutant
822 fold-change under ideal growth-conditions (FC-HS/FC-Growth), with the smallest and
823 largest values indicating the largest mutant growth-differentials between the two screens
824 (smallest PFS_{HS} indicating worse mutant-fitness in the HS-Screen than the Growth-

825 Screen, and largest PFS_{HS} indicating better mutant-fitness in the HS-Screen than the
826 Growth-screen; Fig. S6). Mutants exhibiting (1) poor growth in the HS-Screen (i.e., low
827 FC-HS of < 0.5 based on performance of known HS-Sensitive *pB*-mutant-clones), and
828 (2) comparatively much better growth in the Growth-Screen (i.e., low PFS_{HS} of < 0.25)
829 were classified as HS-Sensitive in pooled phenotypic screens (indicated in red in Fig.
830 1E-F). Mutants exhibiting poor fitness in both the Growth- and HS-Screens (FC-HS < 0.5
831 and PFS_{HS} > 0.25) are indicated in Fig. 1E-F in yellow (n = 14). These double-sensitive
832 mutants were not included in our "HS-Sensitive" classification to avoid overinterpretation
833 of possibly-confounding phenotypes. We classified mutants displaying a slight growth
834 advantage in response to heat shock (FC-HS > 1.5, n = 28, indicated in the green box,
835 Fig.1E-F) as "HS-Tolerant". Mutants exhibiting neither sensitivity nor tolerance to heat
836 shock were classified as HS-Neutral (n = 49).
837
838 *Assigning drug- and oxidative stress-screen phenotypes*
839 Mutant fold-change in response to the given condition was calculated against an ideal-
840 growth control as above. Mutants in the top 25% of reads recovered in QIseq in the
841 screened condition were classified as Tolerant, while mutants in the bottom 25% were
842 classified as Sensitive.
843
844 *Comparative RNAseq between wild-type NF54 and two HS-Sensitive mutant parasite*
845 *lines in response to heat shock*
846 RNAseq experimental design is outlined in Fig. S8A. Briefly, highly synchronized ring-
847 stage cultures of wildtype NF54 and HS-Sensitive mutants *LRR5* and *DHC* were split
848 equally into four T75 flasks each. All parasites were grown at the normal human body
849 temperature (37C) to early ring-stage. Two flasks of each parasite-line were then
850 exposed to febrile temperatures (41C) for 8 hours, while the remaining two flasks were

851 allowed to continue to grow at 37C for 8 hours without exposure to heat-stress. This
852 temperature-cycling was repeated three times, just as we allowed for the pooled screen.
853 After the third round of heat-shock (Time 1, T^1), RNA was harvested simultaneously from
854 both conditions for RNAseq as in [19]. Parasite fold-change in response to HS was
855 calculated at the time of sample-collection and verified mutant defects in response to HS
856 as compared to NF54 (Fig S8B). RNA-seq was performed in-house on an Illumina
857 MiSeq using a 300-cycle V2 MiSeq reagent kit.
858
859 *RNA-seq data-analysis*
860 RNA-seq reads from each sample were aligned to the P. falciparum reference genome
861 (PlasmoDB version 28, RRID:SCR_013331). A maximum of one mismatch per read was
862 allowed. The mapped reads from TopHat [49] were used to assemble known transcripts
863 from the reference and their abundances were estimated using Cufflinks [50]. The
864 expression level of each gene was normalized as FPKM (fragments per kilobase of exon
865 per million mapped reads). We defined expressed genes as those having FPKM > 20 for
866 at least one biological replicate at either 37°C or 41°C. The fold change of normalized
867 gene expression between 41°C and 37°C was calculated for every biological replicate.
868 Fold-change for genes not expressed in both temperatures was set equal to one. We
869 conservatively filtered out genes in the top and bottom 10% of fold-change to remove
870 outliers. We then fit a Gaussian model to the log2 fold change (*log2FC*) for every
871 biological replicate using maximum log likelihood estimation to normalize the fold-
872 change calculations and assess significance. For each gene *i* with positive fold-change
873 in response to HS, we calculated the p-value as the fraction of genes *g* with $log2FC_g >$
874 $log2FC_i$. For each gene *i* with negative fold-change in response to HS, p-value was
875 calculated as the fraction of genes *g* with $log2FC_g > log2FC_i$. The false discovery rate
876 (FDR) was calculated for each replicate. We defined genes for which FDR < 0.1 as

877 having significant fold-change in response to HS. Genes were assigned HS phenotype-
878 categories based on significance and direction of HS-response. We assigned HS
879 phenotype-categories for 2567 genes using these criteria (Table S3). Heat-shock
880 phenotypes as identified via pooled phenotypic screening and comparative RNAseq
881 were highly correlated (Fig S9A-B), supporting our methodology.
882
883 *GO-term enrichment analyses*
884 All GO-enrichment analyses were performed testing GO-terms mapped to genes in the
885 category of interest against a background of GO-terms mapped to all other genes in the
886 analysis. The GO-term database was created from the latest curated *P. falciparum*
887 ontology available at the time of analysis, downloaded from GeneDB (accessed May 2,
888 2019) [51]. For enrichment-analysis in the 1K-library screens: Mutants were divided into
889 HS-phenotype categories, and each category was tested for enrichment against a
890 background of GO-terms mapped to the genes represented by the remainder of the 922
891 mutants in the screen using the weighted Fisher/elim hybrid-method of the TopGO
892 package (v 1.0) available from Bioconductor [52] (Fig. 2B). For enrichment-analysis in
893 comparative RNAseq data: a database of all GO-terms mapped to the 1298 genes which
894 could be assigned a HS-phenotype in all three parasites was assembled. Genes were
895 divided into HS phenotype-categories based on direction of fold-change (Up, Down,
896 Unchanged) in response to HS in all three parasites, then evaluated for GO-term
897 enrichment against the background GO-term database of all other genes in the analysis
898 using the weighted-Fisher/elim hybrid-method of the TopGO package (Fig 3B, Table
899 S2). For enrichment of apicoplast-targeted genes by RNAseq HS-phenotype category:
900 enrichment for each investigated GO-term g was calculated as the number of non-HS-
901 regulated apicoplast genes C annotated to g (the background-distribution) vs. the
902 number of HS-regulated apicoplast genes C_r annotated to GO-term g. The fraction of

903 HS-regulated apicoplast-genes to non-HS-regulated apicoplast genes (C_r/C) was
904 assessed for significance using the Fisher exact test (Fig 4C).
905
906 **SUPPLEMENTARY FIGURE and TABLE LEGENDS**
907 **Figure S1. Schematic overview of the phenotypic screening pipeline**. *pB*-mutant
908 library resources from small (individual, well-characterized mutant-clones) to large (the
909 1K-Library, comprised of pools randomly selected from the Saturation-Library) were
910 used to design carefully validated pooled screens at increasingly large scale. High
911 correlation between mutant-phenotypes in HS-screens and artemisinin (ART)-screens
912 indicated mechanistic overlap in response to both stressors. Iterative rounds of pooled-
913 screening for various phenotypes over time enables higher-throughput functional-
914 annotation of the *P. falciparum* genome.
915
916 **Figure S2. Extended screening data against the pilot-library and summary.**
917 **A.** Full drug-screening data for artemisinin-compounds Artesunate (AS) and DHA, and
918 proteasome-inhibitor Bortezomib (BTZ) against the pilot-library. HS-Sensitive mutants
919 are significantly more sensitive to each drug than HS-Tolerant mutants. There is no
920 significant relationship between *pB*-mutant sensitivity to any drug and mutant sensitivity
921 in standard growth-conditions.
922 **B.** HS-Sensitive (red) and HS-Tolerant (green) mutants and their phenotypes across all
923 pooled phenotypic screens. Mutants are clustered by HS-phenotype.
924
925 **Figure S3.**
926 Mutants in members of the DV proteome, targets of ART alkylation, and putative
927 interacting partners of K13 tend to be sensitive to HS.

928 **A.** 1k HS-Screen mutants are ordered by FC-HS from HS-Sensitive to HS-Tolerant.
929 Mutants in digestive vacuole-associated proteins as defined by [26] are indicated in
930 lavender dots. Gene-symbols for mutants with HS-sensitivity are labeled with black text
931 (10 of 18 genes). Gene-symbols for HS-Neutral and HS-Tolerant mutants are labeled
932 with grey text.
933 **B.** All mutants in ART alkylation-targets as defined by [9] included in the 1K HS-Screen.
934 **C.** HS-screen phenotypes of mutants in putative K13-interacting proteins as defined by
935 [25].
936
937 **Figure S4.** Core proteasome-components are slightly but universally upregulated in
938 response to HS as compared to other aggregately upregulated processes which have
939 more heterogenous expression. Fold-change for most individual proteasome-
940 components did not meet our threshold to be designated "upregulated". ** Wilcoxon p-
941 value < 1e-5.
942
943 **Figure S5. QIseq data-correlations within and between Pilot-Library Screens. A.**
944 Pearson correlations between 5' and 3' QIseq data for 37°C_ideal-growth screen and
945 41°C_heat-shock screen indicate highly reproducible analyses across technical and
946 biological replicates in both screens.
947 **B.** Correlations within and between 37°C_ideal growth screen and 41°C_heat-shock
948 screen QIseq data. High correlations within both HS-screens and Growth-screens (HS-
949 Screen, R=0.94; Growth-Screen, R=0.89) and weak correlation between HS-screens
950 and Growth-screens (R = ~0.42) suggests heat-shock exposure-conditions were
951 sufficient to allow reproducible detection of mutants with specific selection response-
952 phenotypes from pooled screening.
953

954 **Figure S6. QIseq data-correlations of 1K-Library screening for *P. falciparum* heat-**
955 **shock phenotypes.** 1K-Library screens were as robust and reproducible as the pilot-
956 library screens. QIseq data correlations within and between HS-screens and Growth-
957 screens for a representative pool of the 1K-mutant library are shown.
958
959 **Figure S7. Phenotypic Fitness-Score in HS (PFS_{HS}) distribution across mutant HS**
960 **phenotype-classifications in the 1K-Library screen.** See Table S2 and Methods for
961 PFS_{HS} calculation details. HS-Sensitive mutants (mutants displaying defective growth in
962 response to heat shock but not in response to ideal growth conditions) are assigned the
963 lowest PFS_{HS}, while HS-Tolerant mutations are assigned the highest PFS_{HS}.
964
965 **Figure S8. Methods and validation for comparative RNAseq.**
966 **A.** RNA sample-collection methods for wildtype malaria-parasite NF54 vs. two HS-
967 Sensitive *pB*-mutant clones **Δ*DHC* (PB4) and Δ*LRR5* (PB31)** in response to febrile
968 temperatures. Assays were performed in biological duplicate.
969 **B.** Validation of HS-Sensitive mutant-clones during RNA-Seq Sample preparation**.** Both
970 mutants grown individually had growth-defects in response to HS as compared to NF54.
971
972 **Figure S9. Complementary methods (pooled phenotypic screening, phenotypic**
973 **transcriptional profiling of HS-Sensitive mutants vs. wildtype in response to heat**
974 **stress) indicate genes driving the parasite heat-stress response.**
975 **A**. HS-Sensitive *pB* mutants tend to have mutations in genes that have significant
976 changes in expression in response to heat-stress, while mutants that are neutral to or
977 tolerant of heat-stress tend to have mutations in genes that are not regulated in
978 response to heat-stress.

979 **B**. *pB* mutants in genes normally up-regulated in response to heat-stress grow poorly in
980 response to heat-stress (i.e., have significantly lower phenotypic fitness-scores) than
981 mutants in genes that are neutral or down-regulated in response to heat-stress.
982
983 **Supplemental Tables:**
984 **Table S1. Pooled HS-Screen results of the *P. falciparum pB*-mutant pilot-library (n**
985 **= 128).**
986
987 **Table S2. Pooled HS-Screen results of the 1K-Library (n = 922).**
988
989 **Table S3. Comparative RNAseq-results between NF54 and HS-Sensitive mutant-**
990 **clones *ΔLRR5* and *ΔDHC* in response to heat-shock.**
991 **S3A.** All genes classified into HS response-categories in NF54 with or without exposure
992 to heat-shock using RNAseq data (n = 2567). HS-classifications for each gene in two
993 HS-Sensitive mutant-lines are indicated where available. Criteria for inclusion: NF54
994 expression above threshold (FPKM > or = 20 for at least one replicate in at least one
995 temperature-condition) and FC-HS supported by two biological replicates.
996 **S3B.** Genes included in functional enrichment-analyses. Criteria for inclusion: all genes
997 with expression above threshold AND agreement between replicates as to HS fold-
998 change classification for all three parasite lines (n = 1298).
999 **S3C.** Enriched GO-terms for specified HS-response-categories as included in Figure 3B.
1000 “Annotated”: the number of genes annotated to a given GO-term included in the analysis
1001 for all HS response-categories. “Significant”: the number of genes annotated to a given
1002 GO-term in the HS response-category being tested for enrichment.
1003 **S3D.** Full functional enrichment-results for all HS response-categories.
1004

1005 **Table S4. Drug- and oxidative stress-screen results of the pilot library (n = 128).**

1006

1007

1008 **Table S5. Qlseq dataset accession numbers.**

1009 **References**
1010

1011 1. WHO: **World Malaria Report.** *World Health Organization* 2018.

1012 2. Gardner MJ, Hall N, Fung E, White O, Berriman M, Hyman RW, Carlton JM, Pain
1013 A, Nelson KE, Bowman S, et al: **Genome sequence of the human malaria**
1014 **parasite *Plasmodium falciparum*.** *Nature* 2002, **419:**498-511.

1015 3. Aurrecoechea C, Brestelli J, Brunk BP, Dommer J, Fischer S, Gajria B, Gao X,
1016 Gingle A, Grant G, Harb OS, et al: **PlasmoDB: a functional genomic database**
1017 **for malaria parasites.** *Nucleic Acids Res* 2009, **37:**D539-543.

1018 4. Oakley MS, Gerald N, McCutchan TF, Aravind L, Kumar S: **Clinical and**
1019 **molecular aspects of malaria fever.** *Trends in parasitology* 2011, **27:**442-449.

1020 5. Oakley MSM, Kumar S, Anantharaman V, Zheng H, Mahajan B, Haynes JD,
1021 Moch JK, Fairhurst R, McCutchan TF, Aravind L: **Molecular factors and**
1022 **biochemical pathways induced by febrile temperature in intraerythrocytic**
1023 ***Plasmodium falciparum* parasites.** *Infection and immunity* 2007, **75:**2012-
1024 2025.

1025 6. Zhang M, Wang C, Otto TD, Oberstaller J, Liao X, Adapa SR, Udenze K, Bronner
1026 IF, Casandra D, Mayho M, et al: **Uncovering the essential genes of the**
1027 **human malaria parasite *Plasmodium falciparum* by saturation mutagenesis.**
1028 *Science* 2018, **360**.

1029 7. Rocamora F, Zhu L, Liong KY, Dondorp A, Miotto O, Mok S, Bozdech Z:
1030 **Oxidative stress and protein damage responses mediate artemisinin**
1031 **resistance in malaria parasites.** *PLoS pathogens* 2018, **14:**e1006930-
1032 e1006930.

1033 8. Bridgford JL, Xie SC, Cobbold SA, Pasaje CFA, Herrmann S, Yang T, Gillett DL,
1034 Dick LR, Ralph SA, Dogovski C, et al: **Artemisinin kills malaria parasites by**
1035 **damaging proteins and inhibiting the proteasome.** *Nature Communications*
1036 2018, **9:**3801.

1037 9. Ismail HM, Barton V, Phanchana M, Charoensutthivarakul S, Wong MHL,
1038 Hemingway J, Biagini GA, O'Neill PM, Ward SA: **Artemisinin activity-based**
1039 **probes identify multiple molecular targets within the asexual stage of the**
1040 **malaria parasites *Plasmodium falciparum* 3D7.** *Proceedings of the National*
1041 *Academy of Sciences* 2016, **113:**2080-2085.

1042 10. Mok S, Ashley EA, Ferreira PE, Zhu L, Lin Z, Yeo T, Chotivanich K, Imwong M,
1043 Pukrittayakamee S, Dhorda M, et al: **Drug resistance. Population**
1044 **transcriptomics of human malaria parasites reveals the mechanism of**
1045 **artemisinin resistance.** *Science* 2015, **347:**431-435.

1046 11. Yang T, Yeoh LM, Tutor MV, Dixon MW, McMillan PJ, Xie SC, Bridgford JL,
1047 Gillett DL, Duffy MF, Ralph SA, et al: **Decreased K13 Abundance Reduces**
1048 **Hemoglobin Catabolism and Proteotoxic Stress, Underpinning Artemisinin**
1049 **Resistance.** *Cell Reports* 2019, **29:**2917-2928.e2915.

1050 12. Birnbaum J, Scharf S, Schmidt S, Jonscher E, Hoeijmakers WAM, Flemming S,
1051 Toenhake CG, Schmitt M, Sabitzki R, Bergmann B, et al: **A Kelch13-defined**
1052 **endocytosis pathway mediates artemisinin resistance in malaria parasites.**
1053 *Science* 2020, **367:**51.

1054 13. Bronner IFF, Ottoa TD, Zhang M, Udenze K, Wang CCQ, Quail MA, Jiang RHY,
1055 Adams JH, Rayner JC: **Quantitative Insertion-site Sequencing (QIseq) for**
1056 **high throughput phenotyping of transposon mutants.** *Genome Research*
1057 2016.

1058 14. Balu B, Chauhan C, Maher SP, Shoue DA, Kissinger JC, Fraser MJ, Adams JH:
1059 **piggyBac is an effective tool for functional analysis of the *Plasmodium***
1060 ***falciparum* genome.** *BMC microbiology* 2009, **9:**83.

1061 15. Thomas P, Sedillo J, Oberstaller J, Li S, Zhang M, Singh N, Wang CC, Udenze
1062 K, Jiang RH, Adams JH: **Phenotypic Screens Identify Parasite Genetic**
1063 **Factors Associated with Malarial Fever Response in *Plasmodium***
1064 ***falciparum piggyBac* Mutants.** *mSphere* 2016, **1**.

1065 16. Bushell E, Gomes AR, Sanderson T, Anar B, Girling G, Herd C, Metcalf T,
1066 Modrzynska K, Schwach F, Martin RE, et al: **Functional Profiling of a**
1067 **Plasmodium Genome Reveals an Abundance of Essential Genes.** *Cell* 2017,
1068 **170:**260-272.e268.

1069 17. Gisselberg JE, Zhang L, Elias JE, Yeh E: **The Prenylated Proteome of**
1070 ***Plasmodium falciparum* Reveals Pathogen-specific Prenylation Activity and**
1071 **Drug Mechanism-of-action.** *Molecular & Cellular Proteomics* 2017,
1072 **16:**S54-S64.

1073 18. Suazo KF, Schaber C, Palsuledesai CC, Odom John AR, Distefano MD: **Global**
1074 **proteomic analysis of prenylated proteins in *Plasmodium falciparum* using**
1075 **an alkyne-modified isoprenoid analogue.** *Scientific Reports* 2016, **6:**38615.

1076 19. Gibbons J, Button-Simons KA, Adapa SR, Li S, Pietsch M, Zhang M, Liao X,
1077 Adams JH, Ferdig MT, Jiang RHY: **Altered expression of K13 disrupts DNA**
1078 **replication and repair in *Plasmodium falciparum*.** *BMC Genomics* 2018,
1079 **19:**849.

1080 20. Krishnan KM, Williamson KC: **The proteasome as a target to combat malaria:**
1081 **hits and misses.** *Translational Research* 2018, **198:**40-47.

1082 21. Ng CL, Fidock DA, Bogyo M: **Protein Degradation Systems as Antimalarial**
1083 **Therapeutic Targets.** *Trends in Parasitology* 2017, **33:**731-743.

1084 22. Ariey F, Witkowski B, Amaratunga C, Beghain J, Langlois A-C, Khim N, Kim S,
1085 Duru V, Bouchier C, Ma L, et al: **A molecular marker of artemisinin-resistant**
1086 ***Plasmodium falciparum* malaria.** *Nature* 2014, **505:**50-55.

1087 23. Tilley L, Straimer J, Gnädig NF, Ralph SA, Fidock DA: **Artemisinin Action and**
1088 **Resistance in *Plasmodium falciparum*.** *Trends in parasitology* 2016, **32:**682-
1089 696.

1090 24. Bhattacharjee S, Coppens I, Mbengue A, Suresh N, Ghorbal M, Slouka Z,
1091 Safeukui I, Tang H-Y, Speicher DW, Stahelin RV, et al: **Remodeling of the**
1092 **malaria parasite and host human red cell by vesicle amplification that**
1093 **induces artemisinin resistance.** *Blood* 2018, **131:**1234-1247.

1094 25. Gnädig NF, Stokes BH, Edwards RL, Kalantarov GF, Heimsch KC, Kuderjavy M,
1095 Crane A, Lee MCS, Straimer J, Becker K, et al: **Insights into the intracellular**
1096 **localization, protein associations and artemisinin resistance properties of**
1097 ***Plasmodium falciparum* K13.** *PLOS Pathogens* 2020, **16:**e1008482.

1098 26. Lamarque M, Tastet C, Poncet J, Demettre E, Jouin P, Vial H, Dubremetz JF:
1099 **Food vacuole proteome of the malarial parasite *Plasmodium falciparum*.**
1100 *Proteomics Clin Appl* 2008, **2:**1361-1374.

1101 27. Dogovski C, Xie SC, Burgio G, Bridgford J, Mok S, McCaw JM, Chotivanich K,
1102 Kenny S, Gnädig N, Straimer J, et al: **Targeting the Cell Stress Response of**
1103 ***Plasmodium falciparum* to Overcome Artemisinin Resistance.** *PLOS Biology*
1104 2015, **13:**e1002132.

1105 28. White JK, Handa S, Vankayala SL, Merkler DJ, Woodcock HL: **Thiamin**
1106 **Diphosphate Activation in 1-Deoxy-d-xylulose 5-Phosphate Synthase:**
1107 **Insights into the Mechanism and Underlying Intermolecular Interactions.**
1108 *The journal of physical chemistry B* 2016, **120:**9922-9934.

1109 29. Imlay L, Odom AR: **Isoprenoid Metabolism in Apicomplexan Parasites.**
1110 *Current Clinical Microbiology Reports* 2014, **1:**37-50.

1111 30. Kennedy K, Cobbold SA, Hanssen E, Birnbaum J, Spillman NJ, McHugh E,
1112 Brown H, Tilley L, Spielmann T, McConville MJ, Ralph SA: **Delayed death in the**
1113 **malaria parasite *Plasmodium falciparum* is caused by disruption of**
1114 **prenylation-dependent intracellular trafficking.** *PLOS Biology* 2019,
1115 **17:**e3000376.

1116 31. Howe R, Kelly M, Jimah J, Hodge D, Odom AR: **Isoprenoid biosynthesis**
1117 **inhibition disrupts Rab5 localization and food vacuolar integrity in**
1118 ***Plasmodium falciparum*.** *Eukaryotic cell* 2013, **12:**215-223.

1119 32. Pandey AV, Tekwani BL, Singh RL, Chauhan VS: **Artemisinin, an**
1120 **endoperoxide antimalarial, disrupts the hemoglobin catabolism and heme**

1121 **detoxification systems in malarial parasite.** *J Biol Chem* 1999, **274:**19383-
1122 19388.

1123 33. del Pilar Crespo M, Avery TD, Hanssen E, Fox E, Robinson TV, Valente P,
1124 Taylor DK, Tilley L: **Artemisinin and a series of novel endoperoxide**
1125 **antimalarials exert early effects on digestive vacuole morphology.**
1126 *Antimicrob Agents Chemother* 2008, **52:**98-109.

1127 34. Sussmann RAC, Fotoran WL, Kimura EA, Katzin AM: ***Plasmodium falciparum***
1128 **uses vitamin E to avoid oxidative stress.** *Parasites & vectors* 2017, **10:**461-
1129 461.

1130 35. Mène-Saffrané L: **Vitamin E Biosynthesis and Its Regulation in Plants.**
1131 *Antioxidants (Basel, Switzerland)* 2017, **7:**2.

1132 36. Estévez JM, Cantero A, Reindl A, Reichler S, León P: **1-Deoxy-d-xylulose-5-**
1133 **phosphate Synthase, a Limiting Enzyme for Plastidic Isoprenoid**
1134 **Biosynthesis in Plants.** *Journal of Biological Chemistry* 2001, **276:**22901-
1135 22909.

1136 37. Zhang F, Liu W, Xia J, Zeng J, Xiang L, Zhu S, Zheng Q, Xie H, Yang C, Chen
1137 M, Liao Z: **Molecular Characterization of the 1-Deoxy-D-Xylulose 5-**
1138 **Phosphate Synthase Gene Family in *Artemisia annua*.** *Frontiers in Plant*
1139 *Science* 2018, **9**.

1140 38. Heuston S, Begley M, Gahan CGM, Hill C: **Isoprenoid biosynthesis in**
1141 **bacterial pathogens.** *Microbiology* 2012, **158:**1389-1401.

1142 39. Brunetti C, Guidi L, Sebastiani F, Tattini M: **Isoprenoids and phenylpropanoids**
1143 **are key components of the antioxidant defense system of plants facing**
1144 **severe excess light stress.** *Environmental and Experimental Botany* 2015,
1145 **119:**54-62.

1146 40. Clarke A: **The thermal limits to life on Earth.** *International Journal of*
1147 *Astrobiology* 2014, **13:**141-154.

1148 41. Kobayashi Y, Harada N, Nishimura Y, Saito T, Nakamura M, Fujiwara T, Kuroiwa
1149 T, Misumi O: **Algae sense exact temperatures: small heat shock proteins are**
1150 **expressed at the survival threshold temperature in *Cyanidioschyzon***
1151 ***merolae* and *Chlamydomonas reinhardtii*.** *Genome biology and evolution*
1152 2014, **6:**2731-2740.

1153 42. Li GQ, Arnold K, Guo XB, Jian HX, Fu LC: **Randomised comparative study of**
1154 **mefloquine, qinghaosu, and pyrimethamine-sulfadoxine in patients with**
1155 **falciparum malaria.** *Lancet* 1984, **2:**1360-1361.

1156 43. Kirkman LA, Zhan W, Visone J, Dziedziech A, Singh PK, Fan H, Tong X, Bruzual
1157 I, Hara R, Kawasaki M, et al: **Antimalarial proteasome inhibitor reveals**
1158 **collateral sensitivity from intersubunit interactions and fitness cost of**
1159 **resistance.** *Proceedings of the National Academy of Sciences* 2018, **115:**E6863.

1160 44. Oberstaller J, Zhang M, Wang C: **RNAseq dataset: Malaria-parasite survival**
1161 **of host fever is linked to artemisinin resistance** 2020.

1162 45. Boucher MJ, Yeh E: **Evidence that disruption of apicoplast protein import in**
1163 **malaria parasites evades delayed-death growth inhibition.** *bioRxiv*
1164 2018**:**422618.

1165 46. Ralph SA, van Dooren GG, Waller RF, Crawford MJ, Fraunholz MJ, Foth BJ,
1166 Tonkin CJ, Roos DS, McFadden GI: **Metabolic maps and functions of the**
1167 ***Plasmodium falciparum* apicoplast.** *Nature Reviews Microbiology* 2004, **2:**203.

1168 47. Guggisberg AM, Park J, Edwards RL, Kelly ML, Hodge DM, Tolia NH, Odom AR:
1169 **A sugar phosphatase regulates the methylerythritol phosphate (MEP)**
1170 **pathway in malaria parasites.** *Nature Communications* 2014, **5:**4467.

1171 48. Cyrklaff M, Srismith S, Nyboer B, Burda K, Hoffmann A, Lasitschka F, Adjalley S,
1172 Bisseye C, Simpore J, Mueller A-K, et al: **Oxidative insult can induce malaria-**
1173 **protective trait of sickle and fetal erythrocytes.** *Nature Communications* 2016,
1174 **7:**13401.

1175 49. Trapnell C, Pachter L, Salzberg SL: **TopHat: discovering splice junctions with**
1176 **RNA-Seq.** *Bioinformatics* 2009, **25:**1105-1111.

1177 50. Trapnell C, Williams BA, Pertea G, Mortazavi A, Kwan G, van Baren MJ,
1178 Salzberg SL, Wold BJ, Pachter L: **Transcript assembly and quantification by**
1179 **RNA-Seq reveals unannotated transcripts and isoform switching during**
1180 **cell differentiation.** *Nat Biotech* 2010, **28:**511-515.

1181 51. Logan-Klumpler FJ, De Silva N, Boehme U, Rogers MB, Velarde G, McQuillan
1182 JA, Carver T, Aslett M, Olsen C, Subramanian S, et al: **GeneDB--an annotation**
1183 **database for pathogens.** *Nucleic acids research* 2012, **40:**D98-108.

1184 52. Alexa A, Rahnenfuhrer J, Lengauer T: **Improved scoring of functional groups**
1185 **from gene expression data by decorrelating GO graph structure.**
1186 *Bioinformatics* 2006, **22:**1600-1607.
1187

Figure 1. Pooled screens of an extensively characterized *pB*-mutant clone-library allow robust identification of heat-shock phenotypes

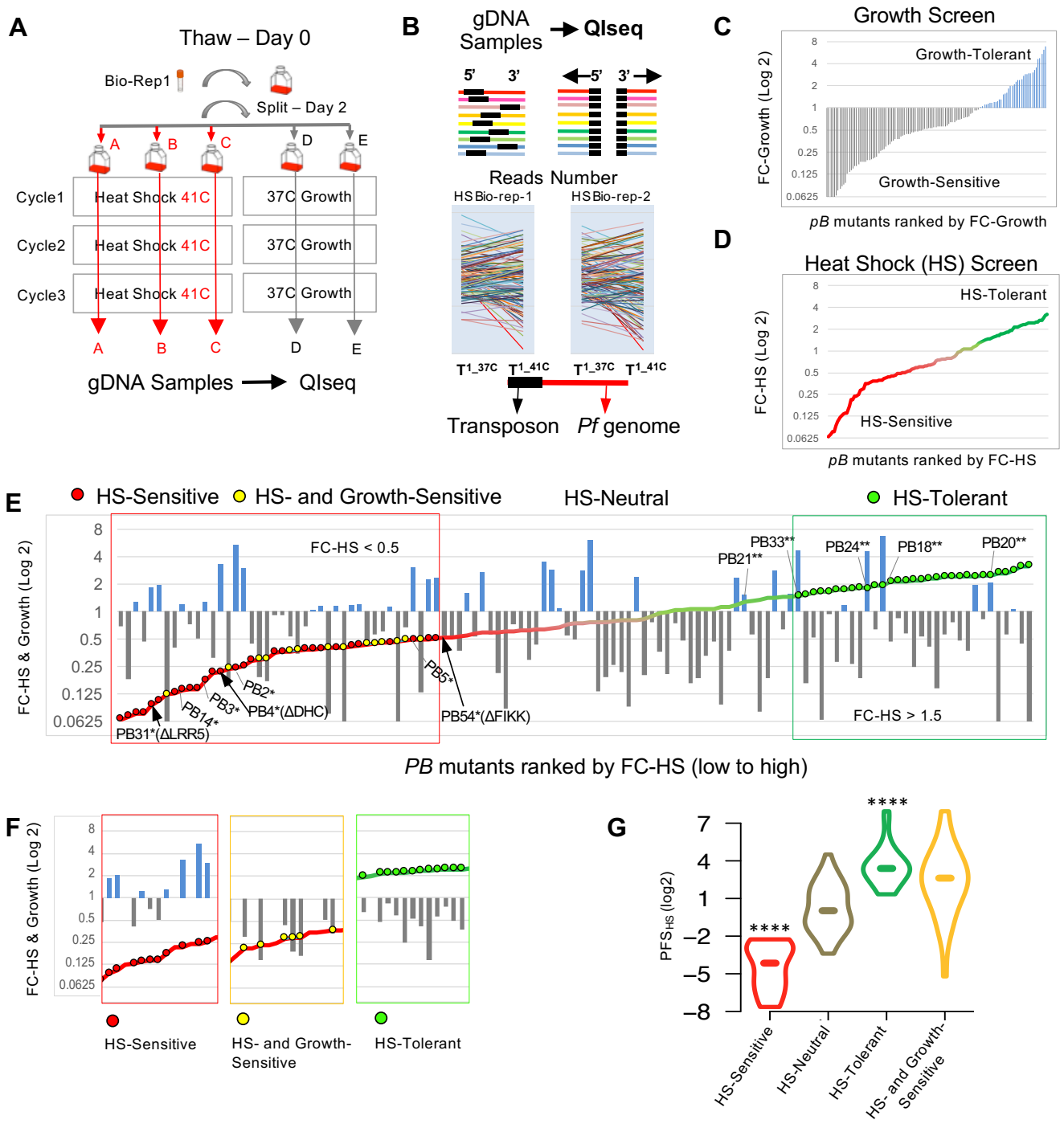

A. Experimental design for pooled heat shock (HS) phenotypic screens. The pilot-library of *pB*-mutant clones (n=128) was exposed to conditions simulating malarial fever. A pilot-library control concurrently grown continuously at 37°C established inherent growth of each *pB*-mutant.
B. QIseq quantifies each *pB*-mutant in the pilot library from sequence-reads of the 5′ and 3′ ends of each *pB* insertion-site. Colored lines represent genes. Black boxes indicate transposon location.
C. Pilot-library mutant growth-phenotypes at ideal temperatures, ranked from Sensitive to Tolerant by FC-Growth. Mutants with inherently slower or faster growth under ideal conditions are shown in grey and blue, respectively.
D. Pilot-library mutant HS-phenotypes ordered from Sensitive (red) to Tolerant (green).
E-F. HS- and Growth-phenotypes of the pilot-library mutants. HS-phenotype of each mutant (displayed as line-graph) is superimposed on its corresponding Growth-phenotype (bar graph). Red = HS-Sensitive mutants (n = 28). Yellow = mutants classified as both Growth-Sensitive and HS-Sensitive (n = 14). Green = HS-Tolerant mutants (n = 30). Mutants neither Sensitive nor Tolerant to HS were classified as HS-Neutral (n = 49). *Known HS-Sensitive *pB*-mutant clones validated by individual HS-assay [15]. **Known HS-Tolerant *pB*-mutant clones validated by individual HS-assay [15].
G. Distributions of PFS_{HS} for mutant HS-phenotype classifications (**** Wilcoxon-test p-value < 1e-15).

Figure 2. **Pooled phenotypic screens scaled up to a 1K *pB*-mutant library enable identification of processes driving the *P. falciparum* heat-shock response**

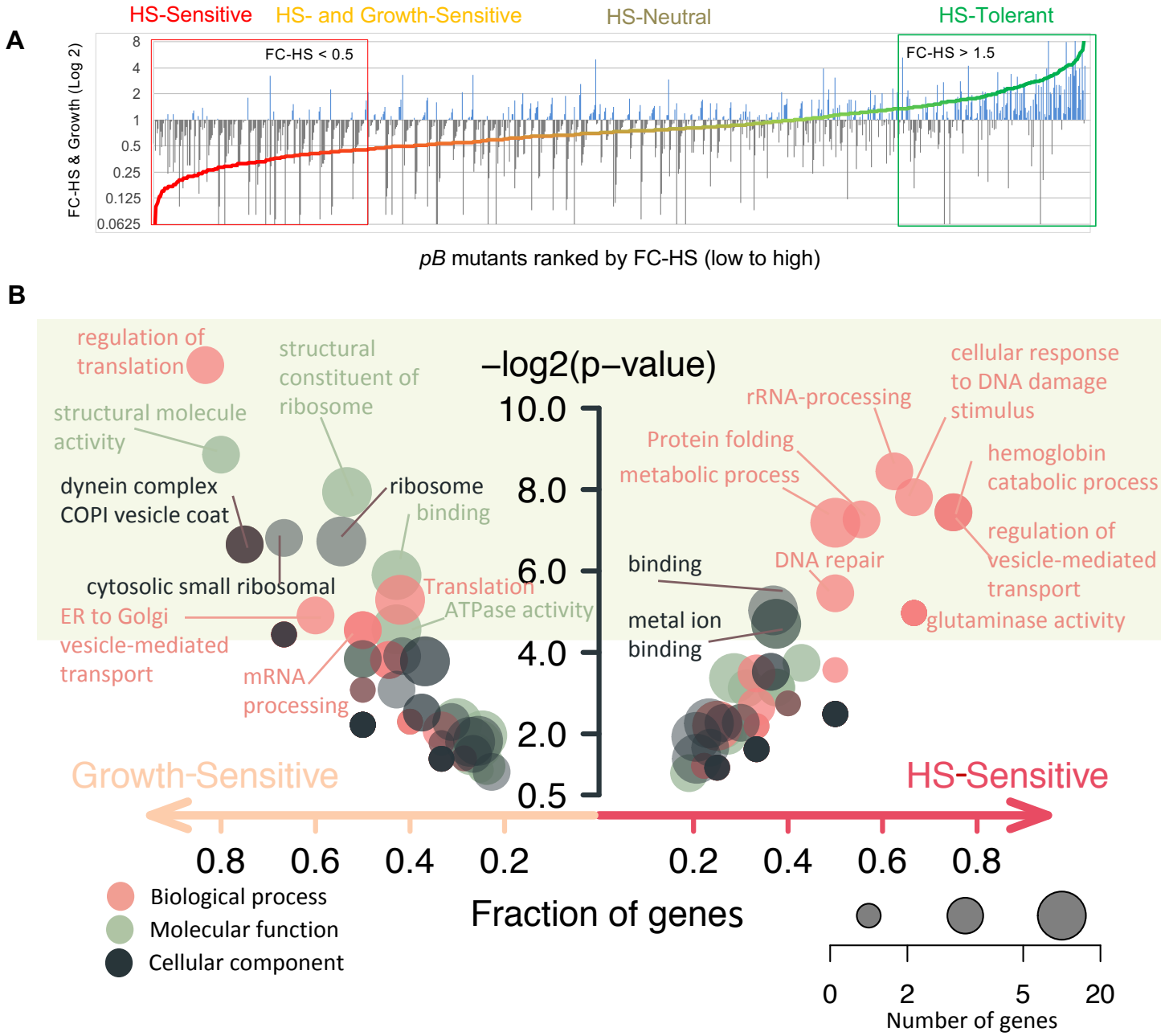

A. HS-Sensitive mutations identified in pooled screens of 922 *pB*-mutants. Mutants are ranked by fold-change in response to HS (FC-HS; n = 922) from HS-Sensitive (red; n = 149) to HS-Tolerant (green; n = 139). Mean mutant fold-change in ideal growth (FC-Growth) is superimposed as a bar plot (gray, FC-Growth < 1.0; blue, FC-Growth > 1.0). Mutants performing poorly in both screens (yellow; n = 91) were classified as HS- and Growth-Sensitive. Mutations neither HS-Sensitive nor HS-Tolerant were classified as HS-Neutral. See Table S2.

B. Functional enrichment of GO terms for HS-Sensitive or Growth-Sensitive *pB*-mutants vs all other mutants in the 1K-library. HS-Sensitive mutants were enriched in terms associated with HS-response such as protein-folding, response to DNA-damage, DNA-repair, and regulation of vesicle-mediated transport. Growth-Sensitive mutants tended to be enriched for more general categories broadly important for survival in all conditions, such as translation- or mRNA-metabolism-related terms. Circles represent GO category, circle color represents ontology, and circle size represents number of significant genes annotated to that category. Significant terms (Fisher/elim-hybrid test p. value <= 0.05) fall within the light-green box.

Figure 3. **Increased transcription of the unfolded protein response, organelle-targeted stress-response pathways and host-cell remodeling characterize the parasite HS-response.**

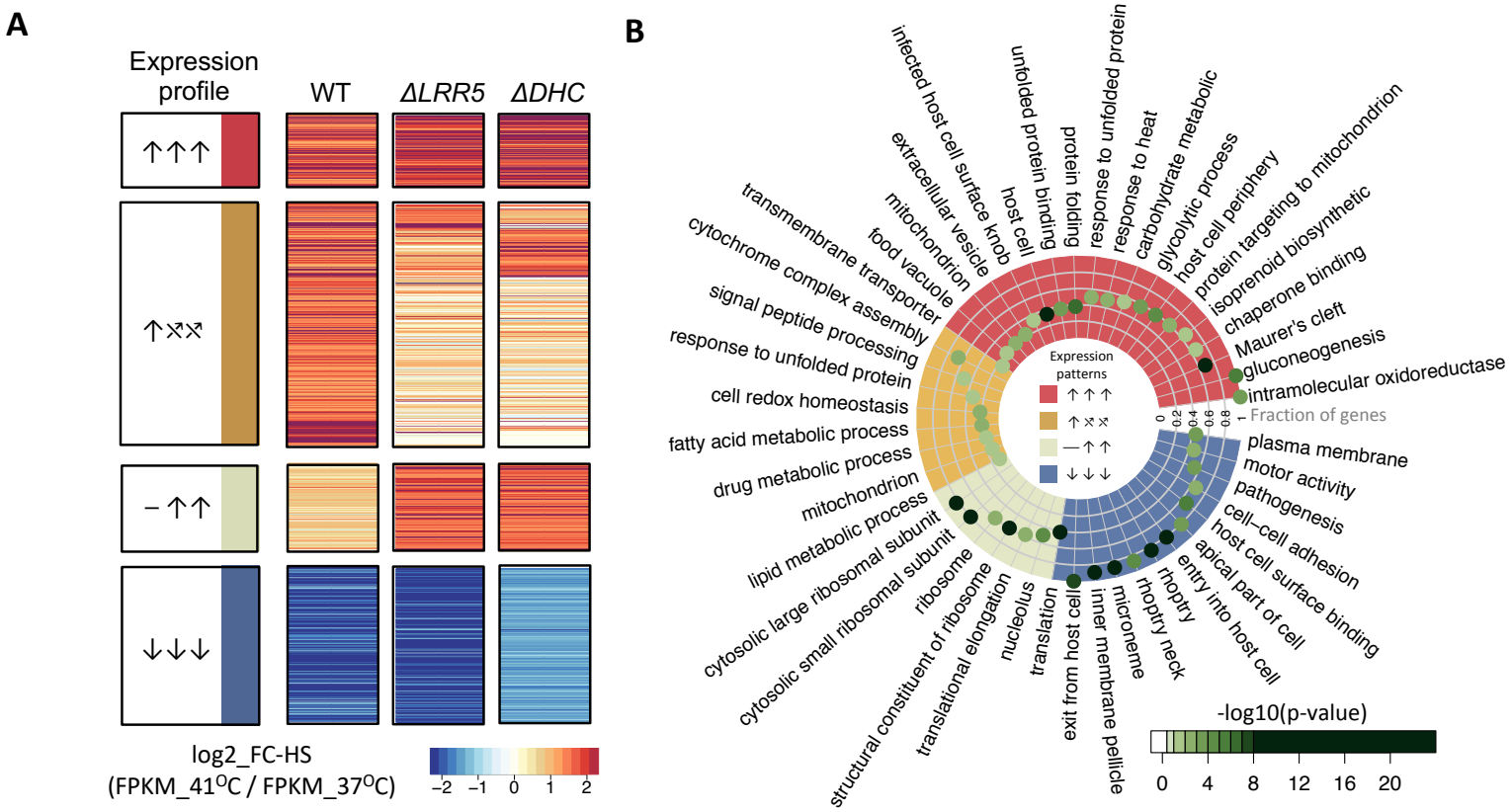

C

Expression profile (HS)	Gene ID	Symbol	Gene Description
↑↑↑	PF3D7_0708400	HSP90	heat shock protein 90
	PF3D7_0209300	IspF	2C-methyl-D-erythritol 2,4-cyclodiphosphate synthase
	PF3D7_1119100*	tRNA-m1G*	tRNA m(1)G methyltransferase, putative
	PF3D7_1037100	PyKII	pyruvate kinase 2
	PF3D7_1439900	TIM	triosephosphate isomerase
	PF3D7_1115700	FP2A	cysteine proteinase falcipain 2a
	PF3D7_0810800	PPPK-DHPS	hydroxymethyldihydropterin pyrophosphokinase…
	PF3D7_1342800	PEPCK	phosphoenolpyruvate carboxykinase
	PF3D7_1129400	NOP2	rRNA (cytosine-C(5))-methyltransferase, putative
	PF3D7_1442500	N/A	geranylgeranyl transferase type-2 subunit …
	PF3D7_0602500	N/A	geranylgeranyltransferase, putative
↑⤮⤮	PF3D7_1337200*	DXS*	1-deoxy-D-xylulose 5-phosphate synthase
	PF3D7_0218300*	N/A	apicoplast RNA methyltransferase (apico-RNA-methyl)
	PF3D7_1239600	ThzK	hydroxyethylthiazole kinase
	PF3D7_1214200	SET5	histone-lysine N-methyltransferase, putative
	PF3D7_1128400	FPPS/GGPPS	geranylgeranyl pyrophosphate synthase, putative
	PF3D7_1437400	PANK2	pantothenate kinase, putative
	PF3D7_1426200	PRMT1	protein arginine N-methyltransferase 1
	PF3D7_1103400	SufD	FeS cluster assembly protein SufD
	PF3D7_0628800	GATB	glutamyl-tRNA(Gln) amidotransferase subunit B
	PF3D7_1443900	HSP90	heat shock protein 90, putative
	PF3D7_1019800	N/A	tRNA methyltransferase, putative
	PF3D7_1450900	N/A	acetyl-CoA acetyltransferase, putative
	PF3D7_0218600	N/A	conserved Plasmodium protein, unknown function

A. (Top-left) HS expression-categories based on phenotype in NF54 vs. HS-Sensitive mutants *ΔLRR5* and *ΔDHC* with and without HS-exposure. HS-regulated genes shared between NF54 and both mutants are indicated in red (↑↑↑) or blue (↓↓↓) for up- and down-regulated genes, respectively. Genes dysregulated in one or both HS-Sensitive mutants fell into two main expression-profile categories underlying mutant HS-Sensitivity phenotypes: those upregulated in NF54 that failed to be regulated in the mutants (↑⤮⤮), and genes not regulated in response to HS in NF54 that were inappropriately upregulated in the mutants (– ↑↑).

B. (Top-right) Functional enrichment analyses between wildtype/mutant HS-expression profiles as defined in A. Red: Shared upregulated HS-responsive GO-terms between NF54 and the two HS-Sensitive *pB*-mutants (↑↑↑). Blue: Shared down-regulated HS-responsive GO-terms (↓↓↓). Ochre: GO-terms upregulated in NF54 but dysregulated in the two *pB*-mutant (↑⤮⤮). Tan: GO-terms enriched in genes not regulated in the wildtype HS-response but upregulated in the mutants (– ↑↑). Only enriched GO-terms are shown (Fisher/elim-hybrid test p. value <= 0.05), with highest significance indicated in dark green. Fraction of significant genes mapping to a GO-term in an HS expression-profile category vs. genes mapping to that GO-term in the entire analysis is indicated by distance to the center of the circle, with the outermost position on the circle indicating 100% of genes in that GO-term are significant. See Table S3D.

C. (Bottom-left) Several apicoplast and isoprenoid biosynthesis-related genes have a tendency to be upregulated in the wildtype-response to HS and are dysregulated in one or both HS-Sensitive *pB*-mutant clones (↑⤮⤮). * Isoprenoid biosynthesis-related genes upregulated by HS confirmed in the pooled HS-screen.

Figure 4. Apicoplast isoprenoid biosynthesis is critical for *P. falciparum* survival of febrile temperatures

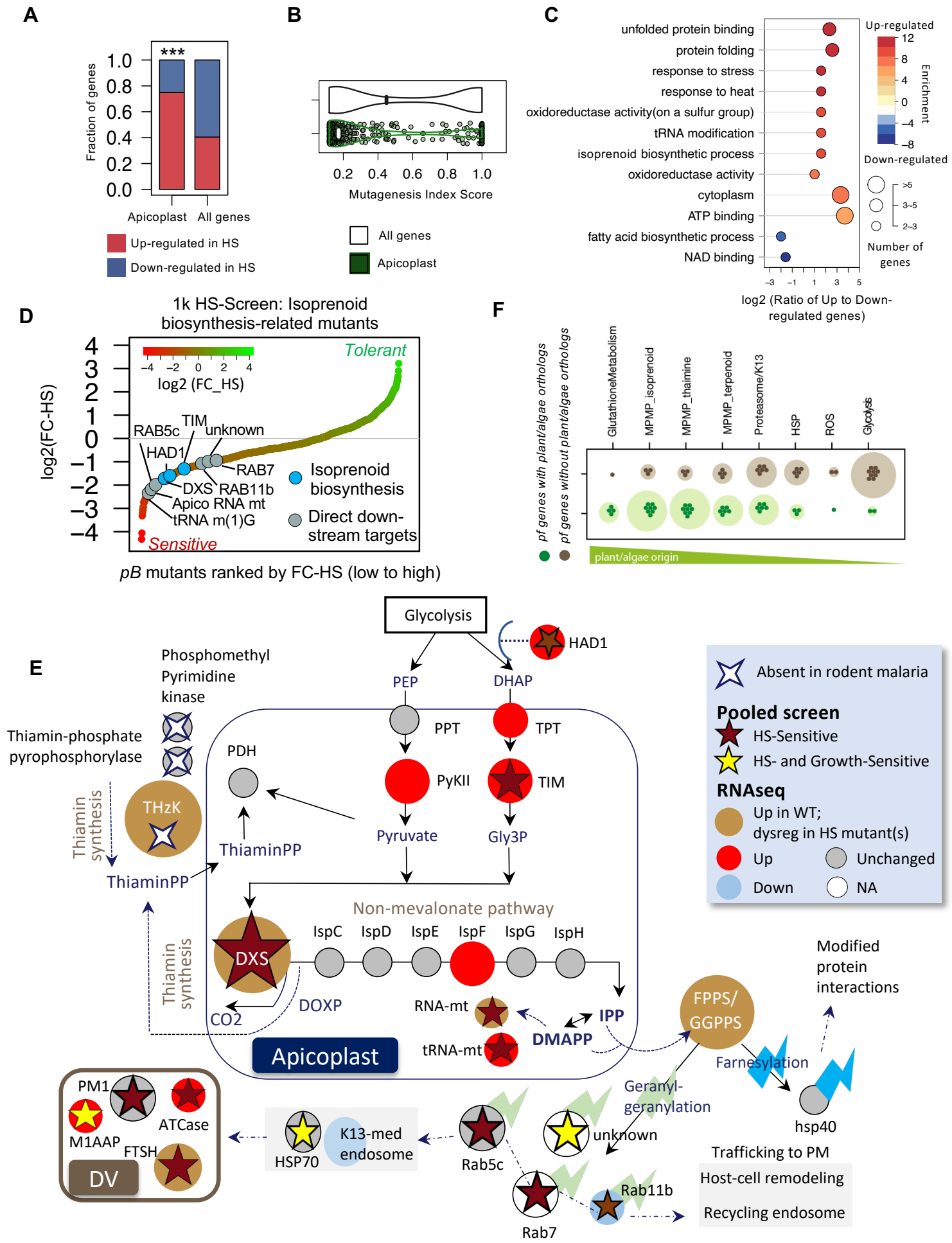

Figure 4. Apicoplast isoprenoid biosynthesis is critical for *P. falciparum* survival of febrile temperatures.

A. Apicoplast-targeted genes tend to be increased in response to HS as compared to all non apicoplast-targeted genes detected above threshold in RNAseq. Apicoplast-targeted genes are as defined in [45] (*** Fisher-test p-value < 1e-5).

B. Apicoplast-targeted genes tend to be highly essential during blood-stage vs. all other non-apicoplast-targeted genes detected above threshold in RNAseq. The median Mutagenesis Index Score (MIS; [6]) for apicoplast-targeted genes is much lower than median MIS for all other genes, indicating a lower tolerance for disruption and thus higher likely essentiality during blood-stage development than non-apicoplast-targeted genes (**** Wilcoxon-test p-value < 1e-15).

C. Apicoplast pathways regulated in response to HS. GO categories enriched in up- and down-regulated apicoplast genes are shown on a scale from red to blue, respectively. The horizontal direction indicates the log ratio between up- and down-regulated apicoplast genes in each category. Circle-size represents gene-number per category.

D. All 8 *pB*-mutants in genes associated with the apicoplast isoprenoid biosynthesis pathway (including direct downstream prenylated targets) represented in the pooled screen were sensitive to heat-shock. Mutants are ranked from HS-Sensitive (red) to HS-Tolerant (green). Circles indicate each HS-Sensitive mutant related to isoprenoid-biosynthesis. See Table S3.

E. Key enzymes in the *P. falciparum* isoprenoid biosynthesis-pathway are up-regulated in response to HS (red circle), dysregulated in HS-Sensitive mutants (ochre) and absent in malaria-parasites of hosts that do not present fever. Pathway diagram modeled from [46]. Isoprenoid biosynthesis-genes upregulated in HS include DXS, 1-deoxy-D-xylulose-5-phosphate synthase (DOXP), 2-C-methyl-D-erythritol 2,4-cyclodiphosphate synthase (IspF), pyruvate kinase II (PyKII), triosephosphate isomerase (TIM), triose phosphate transporter (TPT), and upstream-regulator of MEP-pathway substrates HAD1-phosphotase [47]. All represented Rab GTPases, vesicular trafficking-proteins that are direct downstream-targets prenylated by the MEP-pathway (zigzag) were HS-Sensitive. The key thiamin-synthesis enzyme hydroxyethylthiazole kinase (ThzK) is absent in *P. berghei* and *P. yoelii*, malaria-parasites whose rodent-hosts do not present fever.

F. *P. falciparum* genes with plant orthologs (green circles; n = 1919) indicating potential endosymbiont-ancestry tend to be increased in response to HS vs. genes that do not have plant orthologs (grey circles). The listed processes are sorted based on the ratio of “green” to “non-green” orthologs.

Figure 5. Increased sensitivity to fever is directly correlated with increased sensitivity to artemisinin in the malaria parasite

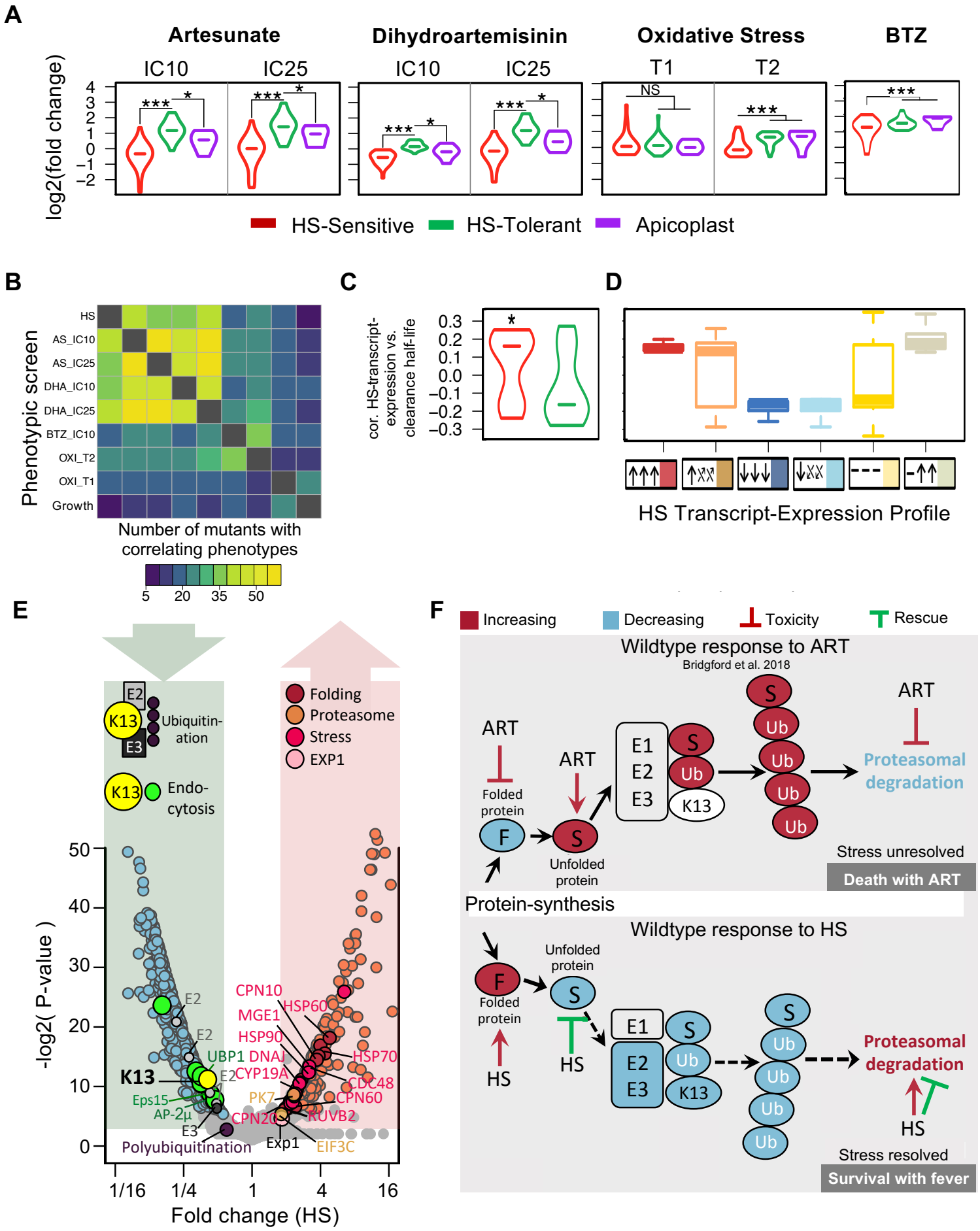

Figure 5. Increased sensitivity to fever is directly correlated with increased sensitivity to artemisinin in the malaria parasite.

A. HS-Sensitive *pB*-mutants (red) are more sensitive to multiple concentrations of artemisinin derivatives AS and DHA, proteasome-inhibitor BTZ, and conditions of heightened oxidative stress than HS-Tolerant parasites (green) in all pooled screens of the pilot library. Apicoplast-mutants (n = 5) have phenotypes similar to all HS-Sensitive mutants (n =28) in artemisinin-derivative screens, but not to proteasome-inhibitors or oxidative stress (* Wilcoxon $p < 0.05$; *** Wilcoxon $p < 1e-10$. See Methods).

B. Correlation between mutant phenotypes in all pooled screens of the pilot library.

C. HS-Sensitive *pB*-mutants (red) are positively correlated with genes linked to ART-R in recent field isolates [10](* Wilcoxon test $p < 0.05$).

D. HS expression-categories as determined by comparative RNAseq between NF54 and two HS-Sensitive mutant clones are positively correlated with ART-R in field-isolates.

E. Both K13-mediated mechanisms of artemisinin resistance (endocytosis, ubiquitin-proteasome system) are similarly regulated in HS. The K13-defined endocytosis pathway (shades of green) and key ubiquitinating-enzymes of the ubiquitin-proteasome system, E2/E3 and K13, are downregulated in the wildtype NF54 HS-response, while protein folding, stress, exported proteins, and proteasome genes are upregulated. RNAseq data are plotted for each gene by average log2 fold-change in response to HS and significance (–log2(p-value)). Circles in shades of blue and pink indicate genes significantly down- or upregulated after exposure to HS, respectively.

F. Activation of pathways underlying DHA-mediated killing and febrile-temperature survival is directly inverse. **Top**: Model of DHA-mediated killing in *P. falciparum* adapted from [8]. Artemisinin (ART) damages and unfolds proteins, prevents folding of newly synthesized proteins, and inhibits the proteasome while at the same time activating E1/E2/E3 ubiquitin-machinery. Accumulation of toxic polyubiquitinated protein-substrates (S) overwhelms the cell and leads to death. **Bottom**: Model of parasite fever-response. Heat-stress causes globally damaged protein. The parasite increases the UPR as it inhibits E2/E3 ubiquitination to prevent accumulation of toxic, polyubiquitinated (Ub) protein-aggregates, while at the same time increasing its capacity for proteasome-mediated degradation—ultimately enabling the parasite to resolve HS-instigated stress and survive febrile-temperatures.